Implementation of a Microgrid Energy Management System Considering E-Mobility, Uncertainties and Contingencies: A Multi-Objective Approach

Derian C. Tairo[a,*], Jéssica Alice A. Silva[a], Juan Camilo López[b], Marcos J. Rider[a]

[a]*Department of System and Energy (DSE), School of Electrical and Computer Engineering (FEEC), State University of Campinas (UNICAMP), Campinas, São Paulo, Brazil*
[b]*Department of Electrical Engineering Mathematics and Computer Science (EEMCS), University of Twente, Enschede, Overijssel, The Netherlands*

Abstract

The integration of various distributed energy resources (DERs), battery energy storage systems (BESSs), photovoltaic (PV) systems, and electric vehicle (EV) chargers, introduces new complexities in managing electrical distribution systems. The main challenge involves devising an optimized day-ahead energy management system (EMS) tailored for three-phase unbalanced AC microgrids while accounting for uncertainties in PV generation and nodal demands. Additionally, the EMS must prepare the microgrid for potential transitions between grid-connected and islanded modes due to unexpected grid outages. The proposed EMS is specifically designed for microgrids comprising PV generation, BESS, EV chargers, and variable demand, facilitating efficient day-ahead planning. Furthermore, the inclusion of contingency constraints ensures a transition between grid-connected and islanded modes, augmenting grid resilience. A multi-objective approach is considered to minimize the operation costs from the main grid and energy non-supplied for the EVs. To evaluate the proposed EMS, actual data from the Campus microgrid (CAMPUSGRID) at the Universidade Estadual de Campinas (UNICAMP) was utilized. The proposed mixed-integer nonlinear programming (MINLP) model undergoes a transformation into a mixed-integer linear programming (MILP) model through a series of linearizations. The model was implemented using Python Optimization Modeling Objects (Pyomo) and solved using the open-source CBC solver. Results confirm the robustness and efficacy of the proposed EMS in improving the performance and resilience of three-phase unbalanced AC microgrids.

Keywords: Energy management systems, electric vehicles, microgrid, multi-objective approach.

1. Introduction

In a world where sustainability and energy efficiency have become global imperatives, effective microgrid management emerges as a revolutionary solution to contemporary energy challenges. Microgrids offer crucial flexibility in integrating renewable energy sources (RESs) and enhancing energy resilience [1]. However, the increasing adoption of electric vehicles (EVs) and the inherent uncertainty in renewable energy generation poses significant challenges for energy management system (EMS). Technologies like Internet of Things (IoT) provide new opportunities to improve the efficiency and adaptability of these systems.

Microgrids are small electrical networks that can operate isolated or connected with the main grid, have emerged as a viable solution for integrating distributed energy resources (DERs), including RESs, battery energy storage systems (BESSs), and controllable loads [2]. In this context, the development and application of mathematical models that incorporate real-time analysis [3, 4], transitions [5], and three-phase systems [6] offer a more accurate and dynamic representation of microgrid behavior.

To address these challenges, it is essential to implement an EMS that can work effectively in microgrids [7, 8]. EMS are designed to monitor, control, and optimize energy use within a microgrid [9], facilitating the integration not only of DERs but also of EVs.

The growing integration of EVs into energy distribution systems [10, 11] has led to the development of several tools and models to manage this integration. However, incorporating EVs into microgrids is crucial for understanding grid impact, enabling energy managers to anticipate and mitigate potential issues such as demand peaks and voltage fluctuations [12]. These models can assess the efficiency of different EV charging and discharging strategies, optimizing the use of available energy resources [13, 14].

A multi-objective optimization approach allows for balancing different priorities, such as, cost reduction, voltage deviation, and efficient EV charging management [24, 15]. The use of multi-objective optimization algorithms [22] in

---
*Corresponding author

Email addresses: `d255905@dac.unicamp.br` (Derian C. Tairo), `j262748@dac.unicamp.br` (Jéssica Alice A. Silva), `j.c.lopezamezquita@utwente.nl` (Juan Camilo López), `mjrider@unicamp.br` (Marcos J. Rider)

Nomenclature

Sets

$\mathcal{B}$	Set of nodes in which a battery energy storage system (BESS) is connected, $\mathcal{B} \subset \mathcal{N}$.
$\mathcal{C}$	Set of contingencies.
$\mathcal{F}$	Set of phases A,B,C.
$\mathcal{G}$	Set of nodes in which a thermal generator (genset) unit is connected, $\mathcal{G} \subset \mathcal{N}$.
$\mathcal{L}$	Set of lines.
$\mathcal{N}$	Set of nodes.
$\mathcal{S}$	Set of scenarios.
$\mathcal{T}$	Set of time intervals.
$\mathcal{V}$	Set of nodes in which electric vehicles (EVs) chargers is connected, $\mathcal{V} \subset \mathcal{N}$.

Indexes

c	Contingency $c \in \mathcal{C}$.
f, h	Phases f and $h \in \mathcal{F}$.
i, j	Nodes $i \in \mathcal{N}$ and $j \in \mathcal{N}$.
ki, ij	Lines $ki \in \mathcal{L}$ and $ij \in \mathcal{L}$.
m	Nodes $m \in \mathcal{B}$.
n	Nodes $n \in \mathcal{G}$.
r	Nodes $r \in \mathcal{V}$.
s	Scenarios $s \in \mathcal{S}$.
t	Time interval $t \in \mathcal{T}$.

Parameters

α^{C}	Load curtailment cost.
α_n^{G}	Constant operational cost of the genset.
α_t^{S}	Cost of energy imported from the main grid.
Δt	Duration of each time step.
Δt_c	Duration of each time contingency.
η^{B}	Efficiency of the BESS.
η^{EV}	Efficiency of the EV.
$\overline{\Delta_n^{\mathrm{G}}}$	Discretization step for the piecewise linearization.
$\overline{E_m^{\mathrm{B}}}, \underline{E_m^{\mathrm{B}}}$	Maximum/Minimum energy capacity of the BESS.
$\overline{E_r^{\mathrm{EV}}}, \underline{E_r^{\mathrm{EV}}}$	Maximum/Minimum energy capacity of the EV.
$\overline{I^{\mathrm{PCC}}}$	Maximum current of the PCC.
$\overline{P_m^{\mathrm{B}}}$	Maximum dis/charging limit of the BESS.
$\overline{P_r^{\mathrm{EV}}}$	Maximum dis/charging limit of the EV charger.
$\overline{P_n^{\mathrm{G}}}, \underline{P_n^{\mathrm{G}}}$	Maximum/Minimum active power of the genset.
$\overline{Q_r^{\mathrm{G}}}, \underline{Q_n^{\mathrm{G}}}$	Maximum/Minimum reactive power of the genset.
$\overline{V_i}, \underline{V_i}$	Maximum/Minimum voltage magnitude.
$\sigma_{i,y}$	Slope of the yth block for the piecewise linearization.
$\tilde{P}_{ij,f,t,c,s}$	Estimated active power flow.
$\tilde{Q}_{ij,f,t,c,s}$	Estimated reactive power flow.
$\tilde{V}_{i,f,t,c,s}$	Estimated value of the voltage magnitude.
Y	Number of discrete blocks for the piecewise linearization.
$E_m^{\mathrm{B}\circ}$	Initial energy of the BESS.
$E_r^{\mathrm{EV}\circ}$	Initial energy of the EV.
$Prob_s$	Probability of scenario.
$P_{i,f,t}^{\mathrm{D}}$	Profile active power load.
P_i^{D}	Nominal active power load.
$P_{i,f,t}^{\mathrm{PV}}$	Profile active power PV generation.
P_i^{PV}	Nominal active power PV generation.
$Q_{i,f,t}^{\mathrm{D}}$	Profile reactive power load.
Q_i^{D}	Nominal reactive power load.
$R'_{ij,f,t}$	Transformed circuit resistance.
S^{sub}	Total capacity of transformers.
t_a	EV time arrival.
t_d	EV time departure.
V^{nom}	Nominal voltage.
$X'_{ij,f,t}$	Transformed circuit reactance.
$Z'_{ij,f,t}$	Transformed circuit impedance.

Continuous Variables

$\Delta_{i,t,c,y}^{\mathrm{P}}$	Values of the yth block used for the piecewise linearization $(P_{ij,f,t,c,s})^2$.
$\Delta_{i,t,c,y}^{\mathrm{Q}}$	Values of the yth block used for the piecewise linearization $(Q_{ij,f,t,c,s})^2$.
$E_{m,t}^{\mathrm{B}}$	Energy of the BESS.
$E_{r,t}^{\mathrm{EV}}$	Energy of the EV.
$P_{ij,f,t,c,s}^{+}$	Positive component for the piecewise linearization of $(P_{ij,f,t,c,s})^2$.
$P_{ij,f,t,c,s}^{-}$	Negative component for the piecewise linearization of $(P_{ij,f,t,c,s})^2$.
$P_{m,f,t}^{\mathrm{B}+}$	Single-phase charging power of the BESS.
$P_{m,t}^{\mathrm{B}+}$	Three-phase charging power of the BESS.
$P_{m,f,t}^{\mathrm{B}-}$	Single-phase discharging power of the BESS.
$P_{m,t}^{\mathrm{B}-}$	Three-phase discharging power of the BESS.
$P_{m,t}^{\mathrm{B}}$	Active power of the BESS.
$P_{r,f,t}^{\mathrm{EV}+}$	Single-phase charging power of the EV charger.
$P_{r,t}^{\mathrm{EV}+}$	Three-phase charging power of the EV charger.
$P_{r,t}^{\mathrm{EV}}$	Active power of the EV.
$P_{n,f,t,c,s}^{\mathrm{G}}$	Active power of genset at phase f.
$P_{n,t,c,s}^{\mathrm{G}}$	Total active power of the genset.
$P_{ij,f,t,c,s}^{\mathrm{L}}$	Active power losses through the circuits.
$P_{i,f,t,c,s}^{\mathrm{PCC}+}$	Positive component for the piecewise linearization of $P_{i,f,t,c,s}^{\mathrm{PCC}}$.
$P_{i,f,t,c,s}^{\mathrm{PCC}-}$	Negative component for the piecewise linearization of $P_{i,f,t,c,s}^{\mathrm{PCC}}$.
$P_{ij,f,t,c,s}^{\mathrm{PCCsqr}}$	Linear variable used to represent $P_{i,f,t,c,s}^{\mathrm{PCC}}$.
$P_{i,f,t,c,s}^{\mathrm{PCC}}$	Active power at the PCC.
$P_{ij,f,t,c,s}^{\mathrm{sqr}}$	Linear variable used to represent $(P_{ij,f,t,c,s})^2$.
$P_{ij,f,t,c,s}$	Active power flow through the circuits.
$Q_{ij,f,t,c,s}^{+}$	Positive component for the piecewise linearization of $(Q_{ij,f,t,c,s})^2$.
$Q_{ij,f,t,c,s}^{-}$	Negative component for the piecewise linearization of $(Q_{ij,f,t,c,s})^2$.
$Q_{n,f,t,c,s}^{\mathrm{G}}$	Reactive power of the genset at phase f.
$Q_{n,t,c,s}^{\mathrm{G}}$	Total reactive power of genset.
$Q_{ij,f,t,c,s}^{\mathrm{L}}$	Reactive power losses through the circuits.
$Q_{i,f,t,c,s}^{\mathrm{PCC}+}$	Positive component for the piecewise linearization of $Q_{i,f,t,c,s}^{\mathrm{PCC}}$.
$Q_{i,f,t,c,s}^{\mathrm{PCC}-}$	Negative component for the piecewise linearization of $Q_{i,f,t,c,s}^{\mathrm{PCC}}$.
$Q_{ij,f,t,c,s}^{\mathrm{PCCsqr}}$	Linear variable used to represent $Q_{i,f,t,c,s}^{\mathrm{PCC}}$.
$Q_{i,f,t,c,s}^{\mathrm{PCC}}$	Reactive power at the PCC.
$Q_{ij,f,t,c,s}^{\mathrm{sqr}}$	Linear variable used to represent $(Q_{ij,f,t,c,s})^2$.
$Q_{ij,f,t,c,s}$	Reactive power flow through the circuits.
$V_{i,t,c,s}^{\mathrm{sqr}}$	Linear variable used to represent $(V_{i,t,c,s})^2$.
$V_{i,t,c,s}$	Voltage magnitude of the nodes.

Binary Variables

$\chi_{i,t,c,s}$	Variable associated with load and PV curtailment.
$\mu_{i,t,c,s}$	Operational state of the genset.
$b_{m,t}^{\mathrm{Ch}}$	Variable associated with the charge of the BESS.
$b_{m,t}^{\mathrm{Dis}}$	Variable associated with the discharge of the BESS.

Table 1: Comparison of the proposed EMS with previous works.

Ref	Constraints			Three-phase power flow	Uncertainty		Real time	EV charging	Multi-objective	GUI[1]	Case study	Implemented with	Mathematical model[*]
	Connected	Islanded	Transition		Demand	PV							
[3]	✓				✓	✓	✓	✓			Experimental Setup	Matlab	Not mencioned
[4]	✓	✓	✓		✓	✓	✓	✓		✓	Real Microgrid	Pyomo	MILP
[5]	✓	✓		✓	✓	✓					Simulation	AMPL	MISOCP
[6]	✓	✓		✓	✓						Simulation	AMPL	MINLP
[7]	✓				✓	✓	✓	✓	✓		Experimental Setup	Matlab	DL
[8]	✓				✓	✓		✓		✓	Experimental Setup	Not informed	MINLP
[12]	✓				✓	✓		✓			Simulation	Matlab	MIQP
[14]	✓	✓			✓	✓		✓			Experimental Setup	Pyomo	MILP
[15]	✓				✓	✓		✓	✓		Simulation	Matlab	ADMM
[16]	✓							✓	✓		Simulation	Not informed	Heuristic
[17]	✓				✓			✓	✓		Simulation	Not informed	Heuristic
[18]	✓				✓	✓	✓	✓		✓	Experimental	Homer Grid	Heuristic
[19]	✓				✓	✓					Simulation	Matlab	Heuristic
[20]	✓				✓	✓		✓			Simulation	Matlab & GAMS	MILP
[21]	✓	✓			✓	✓	✓	✓		✓	Experimental Setup	Matlab/Simulink	Not mencioned
[22]	✓				✓	✓		✓	✓		Simulation	Not informed	Metaheuristic
[23]	✓	✓	✓	✓	✓	✓	✓		✓		Real Microgrid	Pulp	MILP
[24]	✓			✓	✓	✓		✓	✓		Simulation	AMPL	NLP
[25]	✓	✓	✓	✓	✓	✓	✓	✓		✓	Simulation	Homer Pro & AMPL	MILP & Heuristic
This work	✓	✓	✓	✓	✓	✓	✓	✓	✓	✓	Real Microgrid	Pyomo/Python	MILP

[1] Graphical User Interface.
[*] MINLP - Mixed-Integer Nonlinear Programming, MISOCP - Mixed-Integer Second-Order Cone Programming, MILP - Mixed-Integer Linear Programming, DL - Deep Learning, MIQP - Mixed-Integer Quadratic Programming, ADMM - Alternating Direction Method of Multipliers, RL - Reinforcement Learning, NLP - Nonlinear Programming.

microgrid management enable the development of strategies capable of responding to changing demands and operational uncertainties [16, 17]. Despite incorporating multi-objective models, practical implementation in real microgrid environments remains limited, highlighting the need for new tools.

Frameworks like IoT facilitate data collection from various devices, supporting data analysis and decision-making in EMS [18, 21]. IoT integration in EMS enables continuous and detailed monitoring of the microgrid, from energy generation and storage to final consumption [19]. Connected devices can provide real-time data on network operation, environmental conditions, and equipment status [20]. This information is vital for predictive analysis and operational optimization, allowing energy managers to respond quickly to changes and ensure continuous network operation.

In continuation of the work by [23], which considers transitions from an isolated to a connected system or vice versa, a three-phase AC system, real-time operation, and an IoT-based EMS, this work presents several advancements. Unlike the previous work, which did not consider the development of EVs or a multi-objective approach, this work introduces a multi-objective stochastic approach. It aims to minimize network costs and energy non-supplied (ENS) for EVs, considering uncertainties in photovoltaic (PV) generation and demand. We developed six case studies to evaluate the performance of the EMS, all validated with real data from the campus microgrid (CAMPUS-GRID) at the Universidade Estadual de Campinas (UNI-CAMP). The main contributions of this work are:

- A multi-objective optimization problem (MOOP) approach that minimizes operational costs from the main grid and ENS for EVs. The MOOP is addressed using the ϵ-constraint method.

- The adaptability of a new window in the IoT-based EMS, this feature allows EV owners to input their arrival and departure times, enabling the EMS to plan EV charging according to their needs.

- Validation through real-time simulation using HIL, considering contingencies and the operation of EVs.

For a better understanding of the problem, Table 1 summarizes the literature review.

The structure of this paper is organized as follows: Section 1 introduces the challenges and objectives of the study. Section 2 describes the methodology, detailing the multi-objective mathematical model. Section 3, the EMS software architecture is analyzed, including the new window for the EVs. Sections 4 and 5 present the case studies and results. Finally, section 6 concludes the paper, highlighting the main contributions and suggesting future research and development directions.

2. Methodology

Given the unpredictable nature of solar generation, variable demand, and the increasing integration of EVs into microgrids, we face challenges that require adaptable and innovative solutions. To address these challenges, we have developed an efficient EMS. This system combines stochastic analysis of uncertainties for solar generation and demand, three-phase mathematical modeling with constraints to ensure optimal microgrid performance under various conditions, and multi-objective optimization.

2.1. Uncertainty and Contingency Sets

To deal with the uncertainties of the problem, we utilize various profiles for solar generation and demand. We

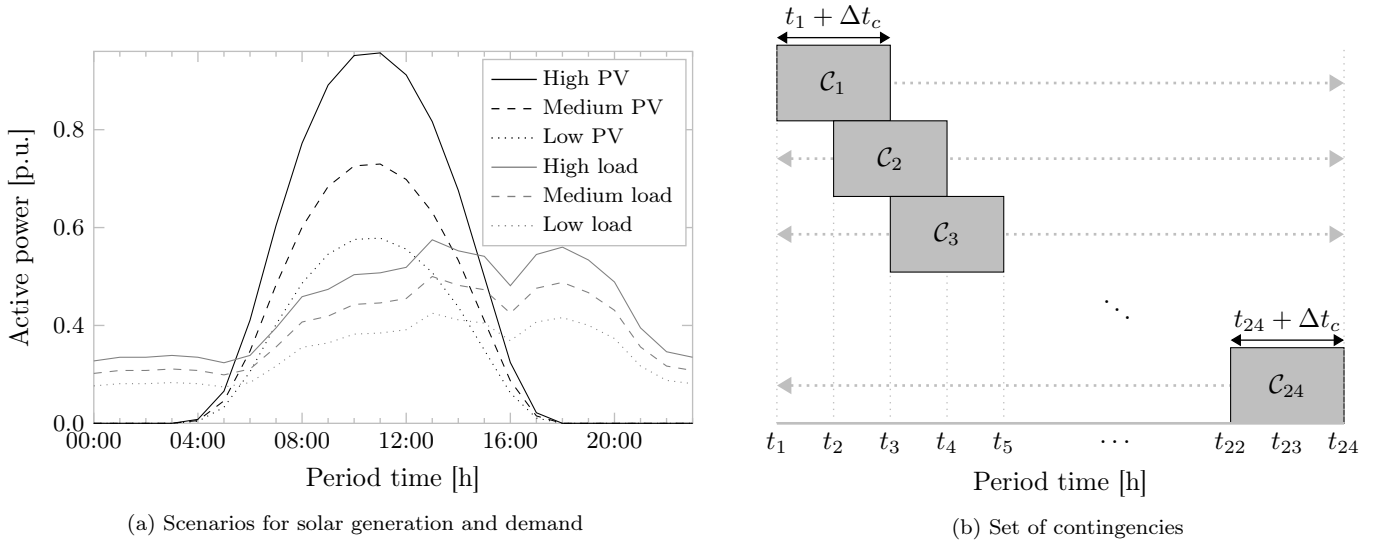(a) Scenarios for solar generation and demand

(b) Set of contingencies

Figure 1: Generation of the set of scenarios (1a) and contingencies (1b).

apply three profiles: high, medium, and low, for both solar generation and demand over a 24-hours period. This results in a total of nine combined scenarios that form the base of the stochastic analysis. Fig. 1a illustrates these scenarios.

Furthermore, failures in the main power grid can occur anytime, forcing the microgrid to operate islanded. In this sense, set $\mathcal{C}$ includes all the possibilities of occurrence of a contingency. The model considers a set of 24 contingencies that reflect all time intervals $\{1, \dots, 24\}$, each potentially occurring at any hour within the 24-hour interval. Each contingency lasts for two hours (Δt_c), after which the microgrid reconnects to the main grid, see Fig. 1b.

2.2. Mathematical Model for the EMS

The EMS mathematical model is formulated as a mixed-integer nonlinear programming (MINLP) model, encompassing two objective functions and constraints related to the three-phase operation of the microgrid under various scenarios and contingencies. The main purpose of the EMS is to find the best solution, minimizing operational costs from the main grid and the ENS for EVs. In sequence, a set of linearizations is used to transform the MINLP into a mixed-integer linear programming (MILP) model, this transformation is detailed in Appendix A.

Into to MILP model, the continuous decision variables are the active and reactive power imported/exported at the point of common coupling (PCC) ($P_{i,f,t,c,s}^{PCC}$, $Q_{i,f,t,c,s}^{PCC}$), the active and reactive power of the genset ($P_{n,t,c,s}^{G}$, $Q_{n,t,c,s}^{G}$), the active power injection of the BESS (P_m^{B}) and the active power injection of the EV (P_r^{EV}).

Moreover, the binary decision variables represent load curtailment and PV disconnection ($\chi_{i,t,c,s}$), as well as the operational state of the genset ($\mu_{i,t,c,s}$). To simplify and reduce the solution time of the optimization problem, a single binary variable is used to denote both load curtailment and PV disconnection. However, it is important to note that this variable does not simultaneously perform load curtailment and PV disconnection, as these actions occur at different nodes within the system.

2.2.1. Objective function 1

The first objective function, given by (1), seeks to minimize the operational costs of the microgrid for a day-ahead scheduling. The first term refers to the cost of purchasing electricity from the main grid. The second term calculates the costs of the diesel generator (genset) operation, and the third term penalizes any load curtailment.

$$f_{costs} = \min \Delta t \sum_{s \in \mathcal{S}} \left\{ Prob_s \cdot \left[\sum_{i \in \mathcal{N}} \sum_{f \in \mathcal{F}} \sum_{t \in \mathcal{T}} \sum_{c \in \mathcal{C}} \alpha_t^{\mathrm{S}} P_{i,f,t,c,s}^{\mathrm{PCC}} \right. \right.$$
$$+ \sum_{n \in \mathcal{G}} \sum_{t \in \mathcal{T}} \sum_{c \in \mathcal{C}} \left(P_{n,t,c,s}^{\mathrm{G}} \cdot \alpha_n^{\mathrm{G}} \cdot \mu_{n,t,c,s} \right)$$
$$\left. \left. + \sum_{i \in N} \sum_{f \in F} \sum_{t \in T} \sum_{c \in C} \alpha^{\mathrm{C}} P_{i,f,t}^{\mathrm{D}} (1 - x_{i,f,t,c}) \right] \right\} \quad (1)$$

2.2.2. Objective function 2

The second objective function, given by (2), aims to minimize the ENS to each EV during the hours that coincides with their departure times. This ensures that the EVs receive sufficient charging, even for intervals of one or two hours, thereby guaranteeing their availability when needed by the EV owner.

$$f_{ens} = \min \sum_{\forall r,t | t = t_d} \left(\overline{E_r^{\mathrm{EV}}} - E_{r,t}^{\mathrm{EV}} \right) \quad (2)$$

4

2.2.3. Constraints related to the operation of three-phase distribution systems

The three-phase unbalanced AC power flow is given by (3)–(11). Constraints (3) and (4) represent the active and reactive power balance in the microgrid. Constraints (5) and (6) calculate the active and reactive power losses at each circuit. Eq. (7) calculates the voltage magnitude through the circuits. Voltage limits are guaranteed by (8), while (9) fixes the voltage magnitude of the PCC node. Current limits are given by (10) and (11) represents the substation capacity.

$$\sum_{ki \in L} P_{ki,f,t} - \sum_{ij \in \mathcal{L}} \left(P_{ij,f,t} + P^{\mathrm{L}}_{ij,f,t} \right) + P^{\mathrm{S}}_{i,f,t} +$$

$$\sum_{n \in \mathcal{G}|i=L^G(n)} P^{\mathrm{G}}_{n,f,t} = P^{\mathrm{D}}_{i,f,t} - P^{\mathrm{PV}}_{i,f,t} +$$

$$\sum_{m \in \mathcal{B}|i=L^B(m)} P^{\mathrm{B}}_{m,t} + \sum_{r \in \mathcal{V}|i=L^{EV}(r)} P^{\mathrm{EV}}_{r,f,t} \quad \forall i,f,t \quad (3)$$

$$\sum_{ki \in \mathcal{L}} Q_{ki,f,t} - \sum_{ij \in \mathcal{L}} \left(Q_{ij,f,t} + Q^{\mathrm{L}}_{ij,f,t} \right) + Q^{\mathrm{S}}_{i,f,t} +$$

$$\sum_{n \in \mathcal{G}|i=L^G(n)} Q^{\mathrm{G}}_{n,f,t} = Q^{\mathrm{D}}_{i,f,t} \quad \forall i,f,t \quad (4)$$

$$P^{\mathrm{L}}_{ij,f,t} =$$
$$\sum_{h \in \mathcal{F}} \frac{1}{V_{i,f,t} V_{i,h,t}} \left[R'_{ij,f,h} \left(P_{ij,h,t} P_{ij,f,t} + Q_{ij,h,t} Q_{ij,f,t} \right) \right.$$
$$\left. + X'_{ij,f,h} \left(Q_{ij,h,t} P_{ij,f,t} - P_{ij,h,t} Q_{ij,f,t} \right) \right] \quad \forall ij,f,h,t \quad (5)$$

$$Q^{\mathrm{L}}_{ij,f,t} =$$
$$\sum_{h \in \mathcal{F}} \frac{1}{V_{i,f,t} V_{i,h,t}} \left[R'_{ij,f,h} \left(P_{ij,h,t} Q_{ij,f,t} - Q_{ij,h,t} P_{ij,f,t} \right) \right.$$
$$\left. + X'_{ij,f,h} \left(P_{ij,h,t} P_{ij,f,t} + Q_{ij,h,t} Q_{ij,f,t} \right) \right] \quad \forall ij,f,h,t \quad (6)$$

$$V^2_{i,f,t} - V^2_{j,f,t} = 2 \sum_{h \in \mathcal{F}} \left(R'_{ij,f,h} P_{ij,h,t} + X'_{ij,f,h} Q_{ij,h,t} \right) -$$
$$\frac{1}{V^2_{i,f,t}} \left[\sum_{h \in \mathcal{F}} \left(R'_{ij,f,h} P_{ij,h,t} + X'_{ij,f,h} Q_{ij,h,t} \right) \right]^2 -$$
$$\frac{1}{V^2_{i,f,t}} \left[\sum_{h \in \mathcal{F}} \left(R'_{ij,f,h} Q_{ij,h,t} - X'_{ij,f,h} P_{ij,h,t} \right) \right]^2 \quad \forall ij,f,h,t \quad (7)$$

$$\underline{V_t} \le V_{i,f,t} \le \overline{V_t} \qquad \forall i,f,t \quad (8)$$

$$V_{i,f,t} = V^{\mathrm{nom}}_t \qquad \forall i,f,t \quad (9)$$

$$\frac{\left(P^2_{ij,f,t} + Q^2_{ij,f,t} \right)}{V^2_{i,f,t}} \le \overline{I}^2_{ij} \qquad \forall ij,f,t \quad (10)$$

$$\left(P^{\mathrm{PCC}}_{i,f,t,c} \right)^2 + \left(Q^{\mathrm{PCC}}_{i,f,t,c} \right)^2 \le \left(\overline{S^{\mathrm{PCC}}} \right)^2 \qquad \forall i,f,t,c \quad (11)$$

2.2.4. Constraints related to genset operation

Eqs. (12)–(15) model the operation of the genset. Constraints (12) and (13) define the total active and reactive power output of each phase, and (14) and (15) impose the active and reactive power limits.

$$P^{\mathrm{G}}_{n,t} = \sum_{f \in \mathcal{F}} P^{\mathrm{G}}_{n,f,t} \qquad \forall n,f,t \quad (12)$$

$$Q^{\mathrm{G}}_{n,t} = \sum_{f \in \mathcal{F}} Q^{\mathrm{G}}_{n,f,t} \qquad \forall n,f,t \quad (13)$$

$$\underline{P^{\mathrm{G}}_n} \cdot u_{n,t} \le P^{\mathrm{G}}_{n,t} \le \overline{P^{\mathrm{G}}_n} \cdot u_{n,t} \qquad \forall n,f,t \quad (14)$$

$$\underline{Q^{\mathrm{G}}_n} \cdot u_{n,t} \le Q^{\mathrm{G}}_{n,t} \le \overline{Q^{\mathrm{G}}_n} \cdot u_{n,t} \qquad \forall n,f,t \quad (15)$$

2.2.5. Constraints related to islanded operation

The proposed formulation considers unexpected outages of the main grid via contingency constraints. In this context, the $\mathcal{C}$ is used to indicate a contingency. Therefore, the security-constrains (16) and (17) model the disconnection of the microgrid to the main grid when $t \ge c$ and $t \le c + \Delta t_\circ$.

$$P^{\mathrm{PCC}}_{i,f,t,c} = 0 \qquad \forall i,f,t,c|_{t \ge c \,\wedge\, t \le c + \Delta t_\circ} \quad (16)$$

$$Q^{\mathrm{PCC}}_{i,f,t,c} = 0 \qquad \forall i,f,t,c|_{t \ge c \,\wedge\, t \le c + \Delta t_\circ} \quad (17)$$

2.2.6. Constraints related to BESS

Constraints (18)–(28) model the operation of the BESS. Note that the BESS do not depend on the set of contingencies $\mathcal{C}$ because the problem finds the optimal operation of the BESS in different operating scenarios. Thus, constraints (18) and (19) defines the state of charge (SoC) of the BESS, where (18) depends on the initial energy of the BESS and (19) depends on the energy stored in the previous period ($E^{\mathrm{B}}_{m,t-1}$). Constraint (20) defines the total input/output power of the BESS considering the respective efficiencies. Constraint (21) guarantees that the BESS do not charge and discharge at the same time. Constraints (22) and (23) define the three-phase dis/charging power, whereas (24) and (25) guarantee a balanced operation. Finally, constraints (26)–(28) specify the limits for the three-phase dis/charging active power, and the energy according to the minimum and maximum capacities, respectively.

$$E^{\mathrm{B}}_{m,t} = E^{\mathrm{B,ini}}_m + P^{\mathrm{B}}_{m,t} \cdot \Delta t \qquad \forall m,t|_{t=1} \quad (18)$$

$$E^{\mathrm{B}}_{m,t} = E^{\mathrm{B}}_{m,t-1} + P^{\mathrm{B}}_{m,t} \cdot \Delta t \qquad \forall m,t|_{t>1} \quad (19)$$

$$P^{\mathrm{B}}_{m,t} = P^{\mathrm{B+}}_{m,t} \cdot \eta^{\mathrm{B}}_m - P^{\mathrm{B-}}_{m,t} \frac{1}{\eta^{\mathrm{B}}_m} \qquad \forall m,t \quad (20)$$

$$P^{\mathrm{B+}}_{m,t} \cdot P^{\mathrm{B-}}_{m,t} = 0 \qquad \forall m,t \quad (21)$$

$$P^{\mathrm{B-}}_{m,t} = \sum_{f \in \mathcal{F}} P^{\mathrm{B-}}_{m,f,t} \qquad \forall m,t \quad (22)$$

$$P^{\mathrm{B+}}_{m,t} = \sum_{f \in \mathcal{F}} P^{\mathrm{B+}}_{m,f,t} \qquad \forall m,t \quad (23)$$

$$P^{\mathrm{B+}}_{m,f,t} = P^{\mathrm{B+}}_{m,h,t} \qquad \forall m,f,h,t \quad (24)$$

$$P^{\mathrm{B-}}_{m,f,t} = P^{\mathrm{B-}}_{m,h,t} \qquad \forall m,f,h,t \quad (25)$$

$$0 \le P^{\mathrm{B+}}_{m,t} \le \overline{P^{\mathrm{B}}_m} \qquad \forall m,t \quad (26)$$

$$0 \le P^{\mathrm{B-}}_{m,t} \le \overline{P^{\mathrm{B}}_m} \qquad \forall m,t \quad (27)$$

$$\underline{E^{\mathrm{B}}_m} \le E^{\mathrm{B}}_{m,t} \le \overline{E^{\mathrm{B}}_m} \qquad \forall m,t \quad (28)$$

2.2.7. Constraints related to EVs

Constraints (29)–(35) model the operation of the EV chargers. Once again, the operation of the EVs does not depend on the set of outages. Thus, constraints (29) and (30) define the state of charge of the EVs. The three-phase charging power is defined by (31) and the balanced injection is enforced by (32). Constraints (33) and (34) specify the limits for the three-phase charging power, and the energy according to the minimum and maximum EV capacities. Eq. (35) imposes that no EV charge is deployed outside t_a and t_d.

$$E_{r,t}^{\mathrm{EV}} = E_r^{\mathrm{EV,ini}} + P_{r,t}^{\mathrm{EV}} \cdot \eta_r^{\mathrm{EV}} \cdot \Delta t \qquad \forall r,t|_{t=t_a} \quad (29)$$

$$E_{r,t}^{\mathrm{EV}} = E_{r,t-1}^{\mathrm{EV}} + P_{r,t}^{\mathrm{EV}} \cdot \eta_r^{\mathrm{EV}} \cdot \Delta t \qquad \forall r,t|_{t>t_a \ \wedge \ t\leq t_d} \quad (30)$$

$$P_{r,t}^{\mathrm{EV}+} = \sum_{f\in\mathcal{F}} P_{r,f,t}^{\mathrm{EV}+} \qquad \forall r,t|_{t>t_a \ \wedge \ t\leq t_d} \quad (31)$$

$$P_{r,f,t}^{\mathrm{EV}+} = P_{r,h,t}^{\mathrm{EV}+} \qquad \forall r,f,h,t|_{t>t_a \ \wedge \ t\leq t_d} \quad (32)$$

$$0 \leq P_{r,t}^{\mathrm{EV}+} \leq \overline{P_r^{\mathrm{EV}}} \qquad \forall r,t|_{t>t_a \ \wedge \ t\leq t_d} \quad (33)$$

$$\underline{E_r^{\mathrm{EV}}} \leq E_{r,t}^{\mathrm{EV}} \leq \overline{E_r^{\mathrm{EV}}} \qquad \forall r,t|_{t>t_a \ \wedge \ t\leq t_d} \quad (34)$$

$$\overline{P_{r,f,t}^{\mathrm{EV}+}} = 0 \qquad \forall r,f,t|_{t<t_a \ \wedge \ t\geq t_d} \quad (35)$$

2.3. Multi-objective Optimization Problem

A MOOP involves more than one objective function to be minimized or maximized, where the answer is a set of solutions defining the best trade-off between the objectives. In this context, dominance determines the solution for the MOOP. For instance, solution x_1 dominates x_2 if x_1 is no worse than x_2 in both objectives and strictly better than x_2 in at least one objective. If either of these conditions is violated, we have non-dominated solutions [26].

Given a set of solutions, the non-dominated solutions are those not dominated by any other solution. This set is called the Pareto-optimal set. The boundary formed by these points is known as the Pareto-optimal front or optimal trade-off surface [27].

To solve the MOOP, we employ the ε-constraint method. This technique is widely recognized for its simplicity and applicability in MOOP [28]. Introduced by [29], this method involves keeping one objective function while restricting the other objectives as constraints within specific values. These values, known as the ε vector, must be chosen within the minimum or maximum values of the constrained objective functions. In this problem, we select the first objective function (1) as the main objective function, and consider the second objective function (2) as a constraint. The modified problem is as follows:

$$\left.\begin{array}{ll} \text{minimize} & f_{costs} \\ \text{subject to} & f_{ens} \leq \varepsilon_p, \\ & (3)-(11),(12)-(15), \\ & (16)-(17),(18)-(28), \\ & (29)-(35) \end{array}\right\} \quad (36)$$

The values of ε_p were chosen based on a range of 20% of the total energy demand of the EVs, including the minimum and maximum values of the objective function (2).

3. EMS Software Architecture

The IoT-based EMS architecture from [23] is used in this work. Unlike previous research, this study introduces a new database table for EVs and includes a new tab in the graphical user interface (GUI) for configuring these EVs. To explain this architecture, it is divided into two parts: the backend and the frontend.

3.1. Backend

The EMS for microgrids consists of five main modules: a stochastic economic dispatch optimizer (EDO) module, an Application programming interface (API), a database, a job scheduler (Cron), and a web-based GUI. The architecture shown in Fig. 2, leverages digital containers to ensure scalability and ease of integration into a microservice architecture. Docker and Docker-Compose [30] are used to build and manage four containers:

- Python-Docker-Container: Runs the EDO, API, and Cron jobs, all developed in Python.

- MySQL-Docker-Container: A relational database for storing historical data and system information.

- Nginx-Docker-Container: An open-source web server for request management.

- Angular-Docker-Container: Hosts and runs the web-based GUI.

The EMS communicates with microgrid internal controllers through a dedicated API (SIL-API), forming a secure RESTful link for exchanging information and controlling actions over the Internet. The Cron module makes HTTP requests to the SIL-API every minute to gather operational data and triggers the EDO module every 24 hours to define a new day-ahead dispatch, which is then sent to the microgrid controllers.

Data on network operations, EDO parameters, and dispatches are stored in the MySQL database. Real-time monitoring and economic dispatch details can be viewed and configured via the web-based GUI. Nginx [31] handles all HTTP requests from the SIL-API, frontend, and API, ensuring efficient and secure data traffic management.

3.1.1. Economic Dispatch Optimizer (EDO)

The main objective of the EDO module is to define the optimal day-ahead scheduling of DER in the microgrid, including the charging and discharging of the BESS, PV and load curtailment, genset dispatch, and EVs charging.

The MOOP mentioned in Section 2.3 is solved using the the solver Cbc [32]. The EDO module is implemented in Python using the Python Optimization Modeling (PYOMO) library [33, 34].

The EDO module is triggered by the Cron module every 24 hours to calculate the optimal dispatch for the next
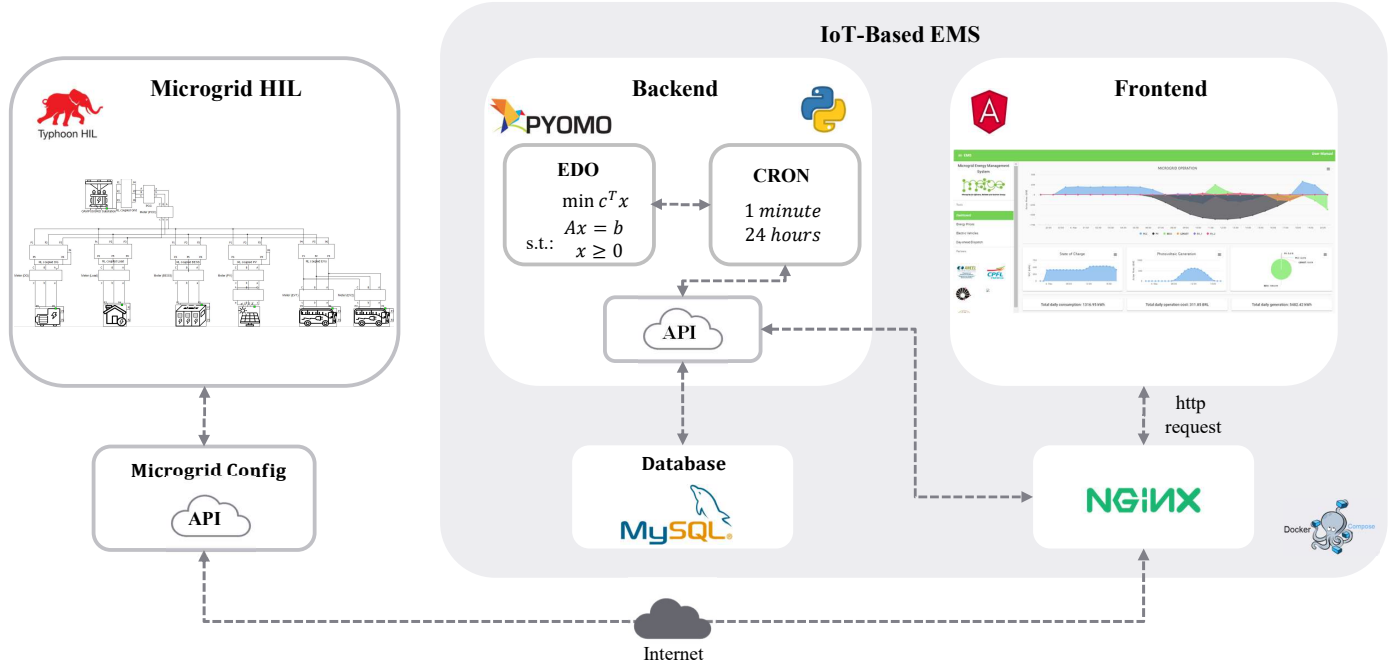
Figure 2: IoT-based EMS for microgrids software architecture.

day. The results are stored in the MySQL database and sent to the microgrid controllers via the SIL-API.

The AC Optimal power flow (OPF) for three-phase unbalanced microgrids is modeled as a MILP problem. The MOOP is solved using the ε-constraint method, where the first objective function minimizes operating costs by considering the cost of electricity from the main grid, genset operation, and load/PV curtailment. The second objective function (ENS for EVs) is constrained. The rest of constraints include power balance, voltage magnitudes, current limits, security constraints, genset operation, BESS operation, and EV charging.

3.1.2. Database

Measured data during microgrid operation, such as nodal voltages, branch currents, power flows, and power injections are stored in a MySQL [35] database. MySQL is an open-source relational database management system, where the user defines the schema, organizes data into tables, and sets rules for relationships between tables.

The proposed database structure is related data into seven tables:

economic_dispatch: Stores dispatch data for the BESS, PV and load curtailment, genset dispatch and EVs charging.

ev_parameters: Contains information on electric vehicles, including arrival and departure times, charging power and battery capacity.

milp_parameters: Contains input parameters for the EDO, such as voltage limits, grid power purchase costs, load curtailment costs, and genset operational costs.

node_information: Stores node details including name,

type of DER, apparent power limits, and SoC limits for the BESS.

branch_information: Contains branch details like name, initial and end nodes, resistance and reactance per phase, and maximum current of the circuit.

node_measurement: Records nodal voltages, active and reactive power injections, and SOC for the BESS node.

branch_measurement: Stores active and reactive power flow values and current in the branches.

The **node_information** table has an one-to-one relationship with the **branch_information** table and an one-to-many relationship with the **node_measurement** table. The **branch_information** table also has an one-to-many relationship with the **branch_measurement** table.

3.1.3. EMS API

The EMS API acts as a connector between the backend and frontend, facilitating communication and integration. Implemented using Flask, a Python web application framework [36], it enables interaction between different parts of the system.

Swagger, a tool for API maintenance, provides a user-friendly interface for testing APIs and visualizing resources. Endpoints such as `/v1/api/ev_information/` are defined within the EMS API, allowing interactions through methods like GET, POST, PUT, and DELETE. These endpoints specify the locations where specific actions can be performed within the system.

3.1.4. SIL-API

In the IoT-based EMS, integration with a simulated microgrid in Typhoon HIL [37] was achieved through the
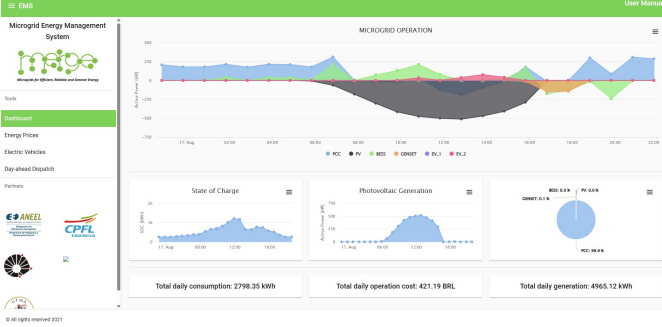
7

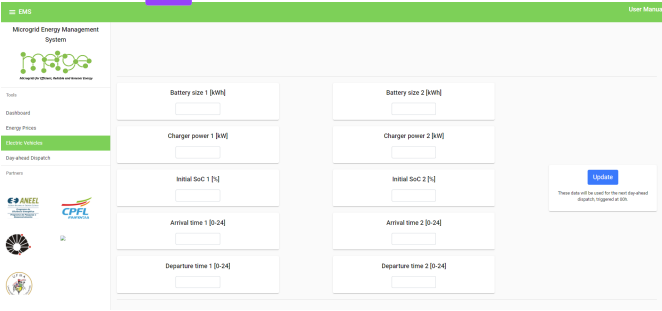Figure 3: GUI of the EMS Frontend.

Figure 4: GUI of the EMS Frontend - EV tab.

SIL-API module [38]. Typhoon HIL allows real-time simulation of microgrids with controllers, controllable via Python scripts. It consists of three components: Microgrid Config, Data Logger, and an API.

The Microgrid Config component controls the simulation process, adjusts simulation status based on dispatch from the EDO, and collects real-time measurements. Data is logged every minute. The API, built with Flask, integrates Microgrid Config with the EMS, providing access to the Data Logger records.

Using the REST architectural style, communication between the microgrid interface and the EMS is independent, ensuring reliability and fast performance. The EMS can be used with various microgrid types, real or simulated, as long as both sides support REST communication.

3.2. Frontend

The frontend of the IoT-based EMS is a user-friendly GUI that allows users to interact with the application through a web browser. It was developed using Angular [39], an open-source software that uses Typescript as its main programming language.

The GUI includes several tabs, each designed to offer specific functionalities. Notably, the EVs tab stands out as it was specifically developed for this work. Fig. 3 shows the GUI of the Frontend. The available tabs are:

- Dashboard: The home screen displays real-time microgrid operation data, including SOC of the BESS, PV power generation, and a pie chart comparing

energy sources. Daily consumption, operation cost, and generation are also shown.

- Electrical Vehicles: Provides information on arrival and departure times, power charging, and battery capacity for EVs, Fig. 4 shows the new EV tab.

- Energy Prices: Users can configure hourly energy prices, thermal generation (genset) costs, and load shedding costs. Configured prices are sent to the database, and a graph displays the changes. For this work, the energy prices were set by [40].

- Day-ahead Dispatch: Shows the dispatch defined by the EDO module for the next day. It includes BESS charge/discharge, load and PV curtailment, and genset dispatch.

4. Case Study

The microgrid was modeled using the schematic editor of Typhoon HIL 604 software [37], with data from a real three-phase AC microgrid deployed on the campus of UNICAMP, São Paulo, Brazil. See Fig. 5. The model includes three-phase impedances and meters for each node. The final node is equipped with an EV charging station, capable of charging one or two EVs simultaneously. The remaining microgrid parameters are detailed in Table 2.

Table 2: Microgrid parameters.

Device	Parameter	Magnitude		Unit
Grid	$\overline{V_i}, \underline{V_i}$	1.05	0.95	[kVA]
	S^{sub}	2375		[%]
	$\overline{I^{\mathrm{PCC}}}$	1000		[A]
	V^{nom}	11.9		[kW]
	P_i^{D}	371		[kW]
	Q_i^{D}	260		[kW]
	P_i^{PV}	736		[kWp]
Genset	$\overline{P_n^{\mathrm{G}}}, \underline{P_n^{\mathrm{G}}}$	150	0	[kW]
	$\overline{Q_n^{\mathrm{G}}}, \underline{Q_n^{\mathrm{G}}}$	150	-150	[kVAr]
	α_n^{G}	30		[m.u.]
BESS	$\overline{P_m^{\mathrm{B}}}, E_m^{\mathrm{B}}$	1275	260	[kWh]
	η^{B}	95		[%]
	$E_m^{\mathrm{B} \circ}$	260		[kWh]
	$\overline{P_m^{\mathrm{B}}}$	1000		[kW]
EV	$\overline{E_r^{\mathrm{EV}}}, \underline{E_r^{\mathrm{EV}}}$	324	64.8	[kWh]
	η^{EV}	95		[%]
	$E_r^{\mathrm{EV} \circ}$	64.8		[kWh]
	$\overline{P_r^{\mathrm{EV}}}$	80		[kW]

The EV charger offers both slow charging (1 plug - 40 kW) and fast charging (using 2 plugs, 40 kW each) [41]. For this study, fast charging is considered. The arrival and departure times (t_a, t_d) at the charging station are set as 1:00 - 7:00 hours for EV 1 and 8:00 - 14:00 hours for EV 2.
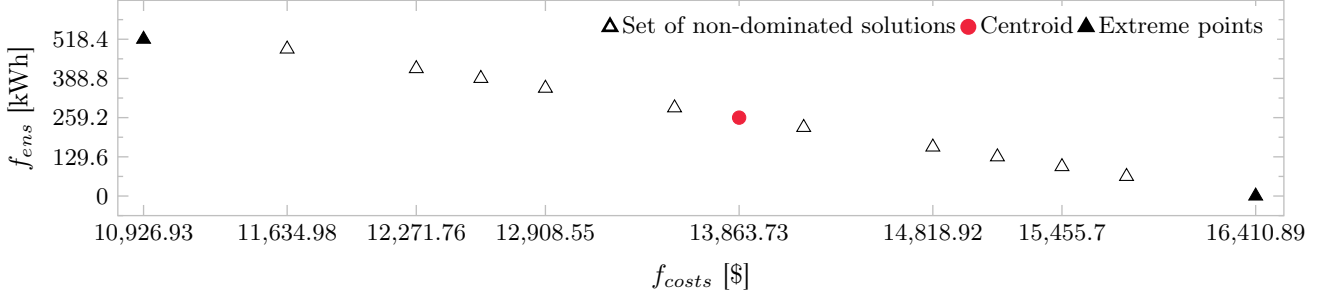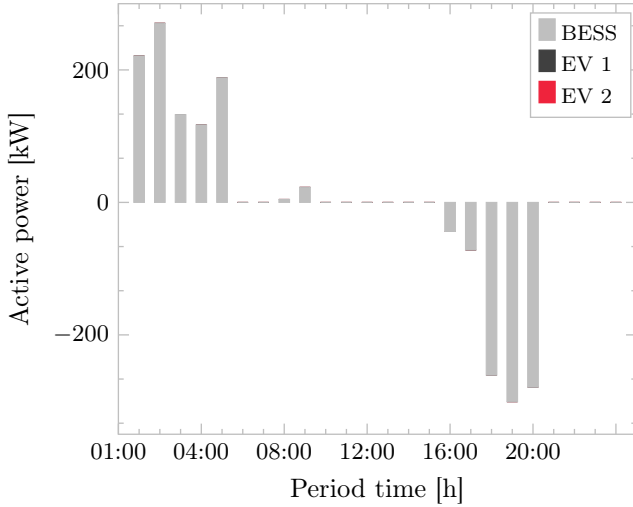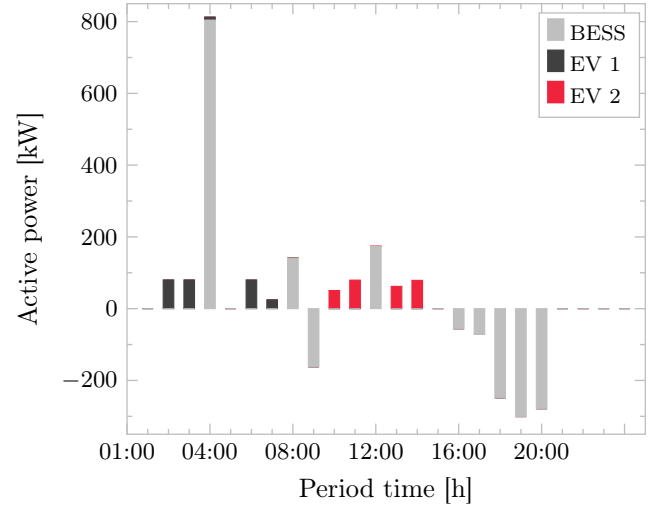
8

Figure 5: Microgrid CAMPUSGRID schematic in Typhoon HIL 604.

To assess the EMS effectiveness in various modes, seven cases were studied:

- Case I: Without contingencies.

- Case II: Contingency at 16:00 hours.

- Case III: Contingency at 08:00 hours.

- Case IV: Without contingencies, including EVs.

- Case V: Contingency at 16:00 hours with EVs.

- Case VI: Contingency at 08:00 hours with EVs.

- Case VII: Contingencies at 08:00 and 16:00 hours with EVs.

To conduct these case studies, the parameters from Table 2 were applied in the backend model and the microgrid simulation in Typhoon HIL 604. Consequently, the results are also reflected in the GUI.

5. Tests and Results

5.1. Multi-objective Analysis

To address the MOOP, the ε-constraint method was applied. Using the Algorithm 1, it obtains the set of non-dominated solutions, forming the Pareto front, as shown in Fig. 6. This algorithm considers nine scenarios and two contingencies at 08:00 and 16:00 hours, respectively. Moreover, the extreme points and the centroid of the Pareto front were analyzed in this study.

For each point, the stochastic EDO determined one optimal day-ahead dispatch of the BESS and EVs for the nine scenarios and two contingencies. The first extreme point represents the solution with the maximum value of f_{ens} and the minimum value of f_{costs}, while the second

---

Algorithm 1: ε-Constraint Method for MOOP

Data: Parameters of the MOOP, including scenarios and contingencies

Result: Pareto front

1 **Initialize:** Set of ε_p values;

2 **for** *each ε_p value in the set* **do**

3   **Solve:** (36);

4   **Store:** Non-dominated solutions;

5 **end**

6 **Generate** Pareto front;

7 **Compute:** The centroid of the Pareto front;

---

extreme point represents the solution with the minimum value of f_{ens} and the maximum value of f_{costs}. The BESS and EV dispatches for these two extreme points are illustrated in Fig. 7.

The first point, Fig. 7a, the BESS is dispatched without any EV charging. This occurs because, at this point, $\varepsilon_p = 518.4$, which represents the maximum value of f_{ens}, results in no EV being charged. Moreover, the minimum value of $f_{costs} = 10,926.93$ indicates that no additional costs are incurred from charging the EVs.

In contrast, at the second extreme point, Fig. 7b, shows the dispatch of both, the BESS and EVs. In this case, $\varepsilon_p = 0$ represents the minimum value of f_{ens}, meaning that both EVs are charged to 100%. This point is associated with a maximum value of $f_{costs} = 16,410.89$, reflecting the higher costs due to the full charging of the EVs. In conclusion, higher EV charging leads to higher operational costs.

Analyzing the extreme points shows that neither solution favors both objective functions. For this reason, the centroid of the Pareto front is calculated, representing the best compromise between the two objectives.

Figure 6: Pareto front

(a) Dispatch for the first extreme point

(b) Dispatch for the second extreme point

Figure 7: Dispatch of the BESS and EVs for the first and second extreme points.

Fig. 6 illustrates this centroid, identified by the pair of values $f_{ens} = 259.2$ kWh and $f_{costs} = 13863.73$ \$. This solution ensures that at least one EV is charged to 100% of its capacity. In this case study, the initial SoC is 64.8 kWh (20%). By adding 259.2 kWh, it guaranteed that the EV reaches its total maximum energy capacity of 324 kWh (100%).

5.2. Results of Case Studies

For the following case studies, the centroid of the Pareto front was adopted as the ε_p value. This value was used to solve the MOOP for seven distinct cases. For each case, the stochastic EDO determined one optimal day-ahead dispatch of the BESS and EV for the nine scenarios. The results of the BESS, genset dispatch, PV curtailment, and EVs are presented in Fig. 8 through Fig. 12, respectively. In addition, the microgrid's 24-hour operation, the SoC of the BESS, and the PV generation are visualized in Figs. 13, 14, and 15 respectively.

Case I represents the normal operation of the microgrid without any contingencies. The optimal dispatch of the BESS takes advantage of the PV generation to charge during the high PV and discharge during the high energy cost periods. Fig. 8a shows the BESS dispatch, while Fig. 13a illustrates the microgrid's 24-hours operation. Figs. 14a and 15a display the SoC of the BESS and PV generation, respectively.

In the second case, the BESS charged at 01:00 and 13:00 hours, almost reaching its total capacity, see Fig. 8b and 13b. This aimed to prepare for the contingency (two hours of duration) and supply the demand along with the genset dispatch. Before the contingency, PV generation supplied the demand. During the contingency, there was PV curtailment in the first hour, as shown in Fig. 10a. Although the BESS was almost fully charged, during the contingency, the PV generation was disconnected, and the generator was operated to supply the demand, as the BESS dispatch is unique for the nine scenarios of the stochastic analysis. This operation is illustrated in Fig. 13b.

Unlike the second case, the third case in Fig. 8c shows the charge of the BESS reached the 25% of its capacity, for discharge during the contingency and supply the demand along with the genset dispatch. After the contingency, the BESS utilizes the PV generation to charge and discharge during the high-cost energy periods. The operation of the microgrid is shown in Fig. 13c.

10

Cases II and III are similar and present one contingency at 16:00 and 08:00 hours, respectively. Both cases show genset dispatch and PV curtailment, as shown in Figs. and 10. It is important to mention that during the contingency, the BESS act like grid forming, controlling the voltage and frequency of the microgrid.

Case IV, similar to the first case, shows the operation of the microgrid without contingencies but includes EVs. Using $\varepsilon_p = 259.2$ and considering the arrival and departure times of the EVs from Section 4, the EDO dispatched only one EV, in this case, the second EV, as shown in Fig. 11a. The EDO prioritizes this EV because it can take advantage of the solar energy available during the day, reaching a ENS equal to 0 (100%). The operation of the microgrid, SoC of the BESS and PV operation is illustrated in Figs. 13d, 14d and 15d respectively.

The fifth and sixth cases are similar to the second and third cases but with the inclusion of EVs. The BESS dispatch, genset and PV curtailment for cases V and VI are shown in Figs. 8e, 8f, 9c, 9d, 10c and 10d, respectively. The analysis of the second and third cases for the genset dispatch and PV curtailment is valid for the fifth and sixth cases. The operation of the microgrid, SoC of the BESS and PV operation is shown in Figs. 13e, 13f, 14e, 14f, 15e and 15f respectively.

The EDO determined that one EV charge in cases IV and V, even though both EVs were included in these scenarios. However, it is important to note that in case VI, the EDO determined the charge both EVs. Regarding the ENS, both EVs reached 50% of their charge, indicating that the EDO can charge either one or both EVs. This occurs because the centroid ($\epsilon = 259$) was adopted.

Case VII, includes two contingencies at 08:00 and 16:00 hours, respectively. The BESS dispatch, genset and PV curtailment are shown in Figs. 16a, 16b, and 16c, respectively. The operation of the microgrid is illustrated in Fig. 16e.

The demand for the first contingency was supplied by the BESS and PV generation, while the second contingency was supplied by the BESS and the genset, there was PV curtailment to maintain the power balance. In contrast to the Fig. 7b, where both EVs was charged, in this case, only one EV was charged, as shown in Fig. 16d, this is due to the ε_p value adopted in the EDO that charge at least one EV to 100% of its capacity.

In summary, in grid-connected operations without contingencies (Case I and Case IV), the BESS charges during the day, leveraging solar energy when costs are lower. Contingencies in Cases II, III, V, VI and VII, the BESS presents a single optimal operation defined in the face of a stochastic analysis, it is possible to observe that in cases where there was a contingency, it was more economically advantageous to dispatch the genset and perform PV curtailment the demand in these rare moments and leave the BESS prepared for discharge in peak periods.

6. Conclusions

A multi-objective optimization problem (MOOP) has been proposed to minimizes the operational costs from the main grid and the energy non-supplied (ENS) for electric vehicles (EVs). The ε-constraint method was applied to solve the MOOP and obtain the Pareto front. The centroid of the Pareto front was used to determine the optimal dispatch of the battery energy storage system (BESS) and EVs for seven case studies.

A new tab and database table for EVs was developed in the IoT-based energy management system (EMS). This tab allows the user to input the EV parameters, such as the arrival and departure times, the maximum energy capacity, and the EV charging power.

All case studies were conducted using the Typhoon HIL 604 and the results were displayed in the GUI. The BESS dispatch, genset dispatch, photovoltaic (PV) curtailment, and EV charging were analyzed for each case. The microgrid's 24-hour operation, the state of charge (SoC) of the BESS, and the PV generation were also visualized.

Appendix A. Piecewise Linearization

The quadratic terms $(P_{ij,f,ht,c})^2$, $(Q_{ij,h,t,c})^2$, $(P_{i,f,t,c}^{\mathrm{PCC}})^2$ and $(Q_{i,f,t,c}^{\mathrm{PCC}})^2$ in (10) and (11) are linearized using a linear piecewise approximation function as presented in [42]. To linearize the terms $(P_{ij,f,ht,c})^2$, $(Q_{ij,h,t,c})^2$, $(P_{i,f,t,c}^{\mathrm{PCC}})^2$ and $(Q_{i,f,t,c}^{\mathrm{PCC}})^2$, the variables $(P_{ij,f,ht,c}^{sqr})^2$, $(Q_{ij,h,t,c}^{sqr})^2$, $(P_{i,f,t,c}^{\mathrm{PCCsqr}})^2$ and $(Q_{i,f,t,c}^{\mathrm{PCCsqr}})^2$ is introduced to the model the square of the active and reactive power flow and square of the active and reactive power at the PCC. Therefore, constrains related to the definition of variables and their limits for the piecewise linearization approximation are given in (A.1)-(A.6).

$$f(x,\overline{x},Y) = \sum_{y=1}^{Y} \sigma_{x,y} \cdot \Delta_{x,y} \quad \forall x \tag{A.1}$$

$$x = x^{+} - x^{-} \quad \forall x \tag{A.2}$$

$$x^{+} - x^{-} = \sum_{y=1}^{Y} \Delta_{x,y} \quad \forall x \tag{A.3}$$

$$0 \le \Delta_{x,y} \le \overline{x}/Y \quad \forall x, y = 1, \ldots, Y \tag{A.4}$$

$$\sigma_{x,y} = (2y-1)\overline{x}/Y \quad \forall x, y = 1, \ldots, Y \tag{A.5}$$

$$x = x^{+} - x^{-} \ge 0 \tag{A.6}$$

*Appendix A.1. Linearization of the AC power flow model*

The definition of the apparent power losses in (5) and (6) is nonlinear due to multiplication of continuous variables. To linearize these constraints, estimated active and reactive power flows through lines of each phase f, i.e., $\tilde{P}_{ij,h,t} P_{ij,f,t}$ and $\tilde{Q}_{ij,h,t} Q_{ij,f,t}$ and, the estimated values of voltage magnitudes, i.e., $\tilde{V}_{i,f,t}$ and $\tilde{V}_{i,h,t}$ can be used. Thus, $P_{ij,f,t}^{\mathrm{L}}$ and $Q_{ij,f,t}^{\mathrm{L}}$ can be approximated using the linear expression given by (A.1) and (A.2).
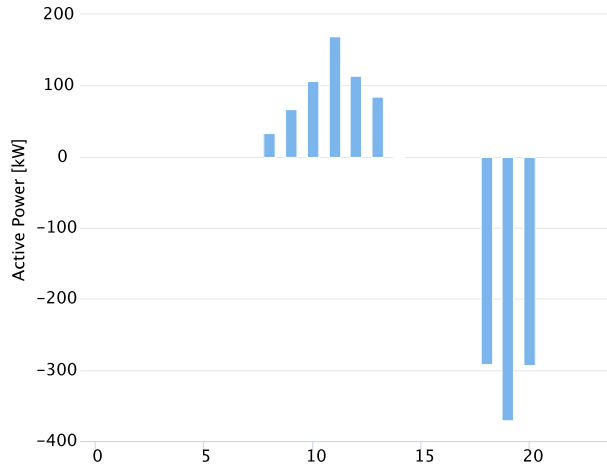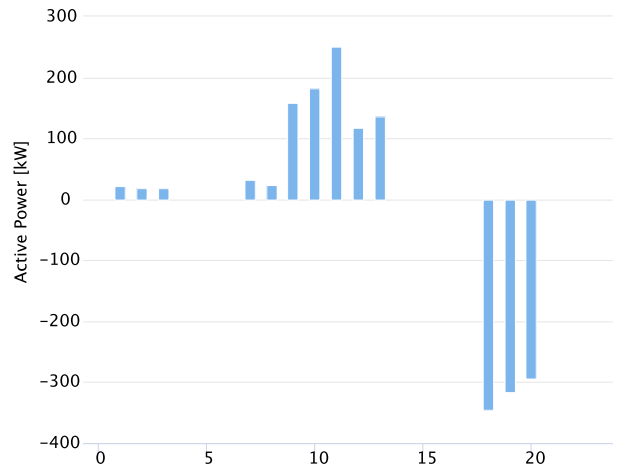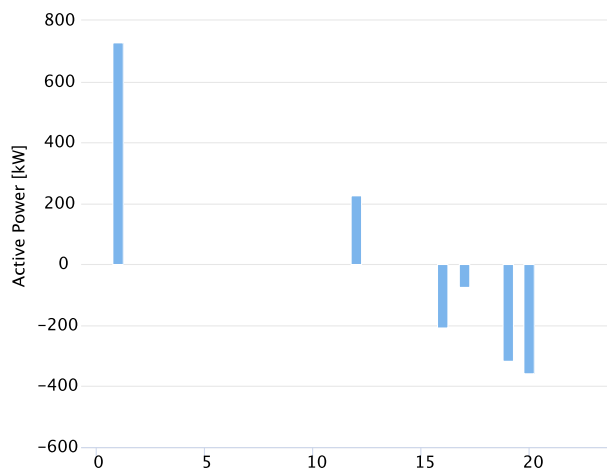
(a) Case I: Without contingencies.
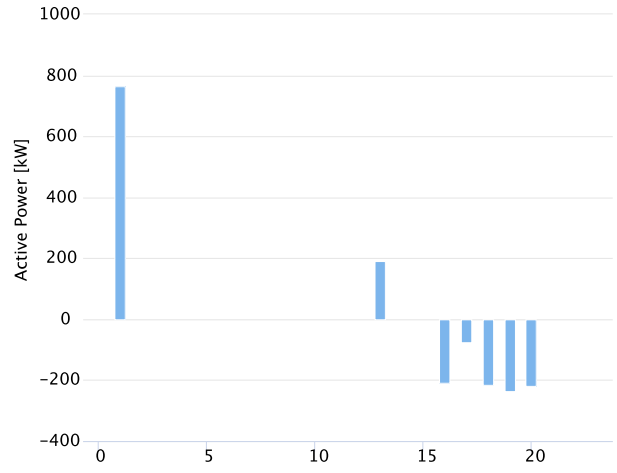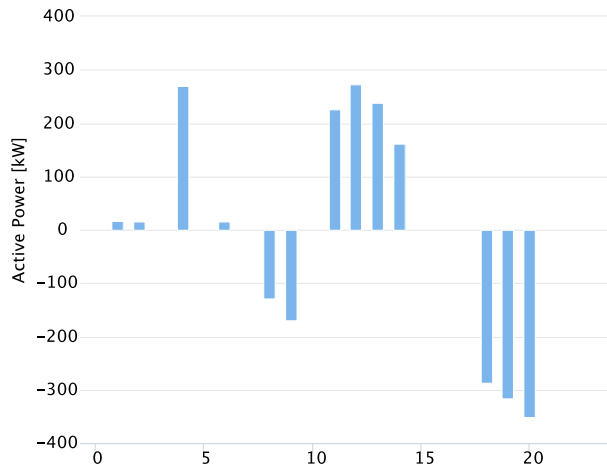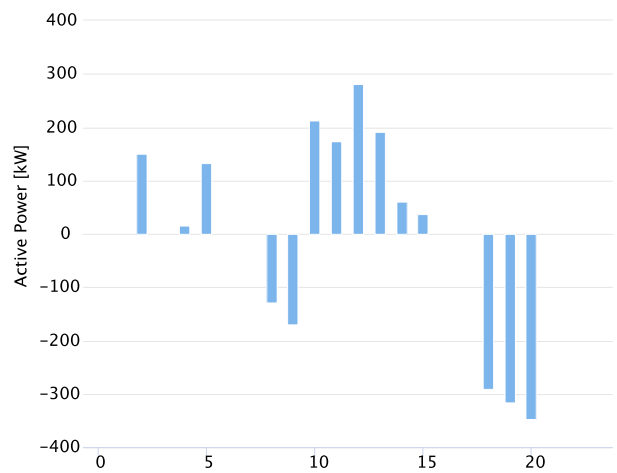
(b) Case II: Contingency at 16:00 hours.

(c) Case III: Contingency at 08:00 hours.

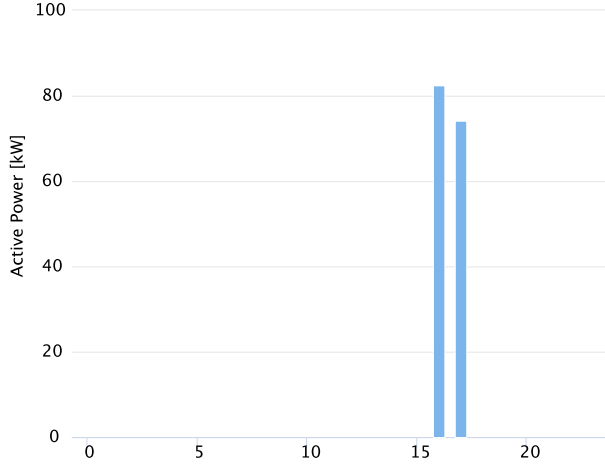(d) Case IV: Without contingencies, including EVs.

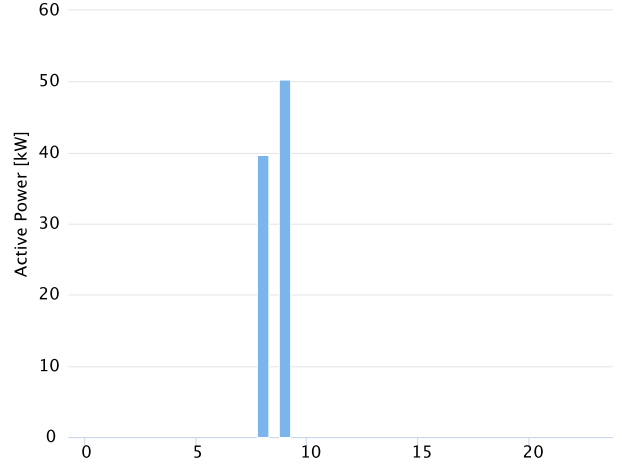(e) Case V: Contingency at 16:00 hours with EVs.

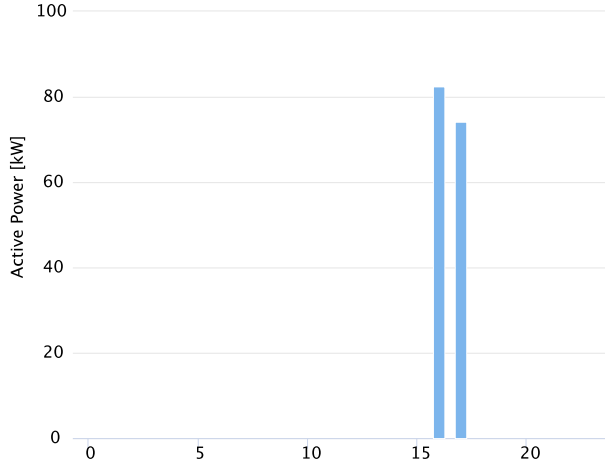(f) Case VI: Contingency at 08:00 hours with EVs.
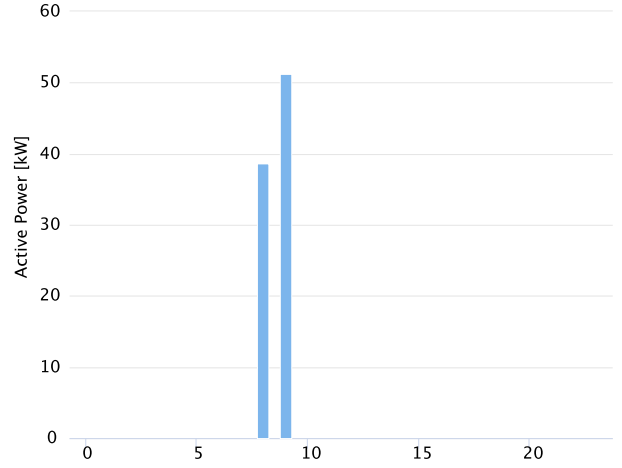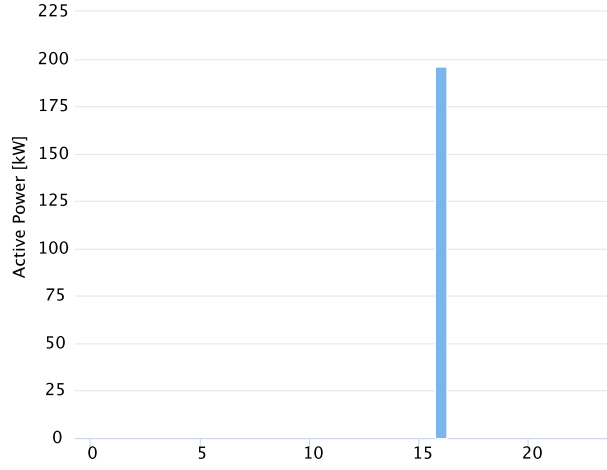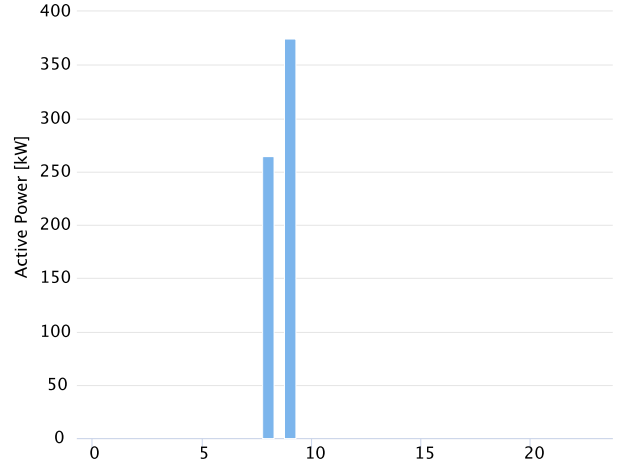
Figure 8: BESS dispatch for each case.

12

(a) Case II: Contingency at 16:00 hours.

(b) Case III: Contingency at 08:00 hours.

(c) Case V: Contingency at 16:00 hours with EVs.

(d) Case VI: Contingency at 08:00 hours with EVs.

Figure 9: Genset dispatch for each case.

$$P^{\mathrm{L}}_{ij,f,t} =$$
$$\sum_{h\in\mathcal{F}} \frac{1}{\tilde{V}_{i,f,t}\tilde{V}_{i,h,t}} \left[R'_{ij,f,h}\left(\tilde{P}_{ij,h,t}P_{ij,f,t} + \tilde{Q}_{ij,h,t}Q_{ij,f,t}\right)\right.$$
$$\left. + X'_{ij,f,h}\left(\tilde{Q}_{ij,h,t}P_{ij,f,t} - \tilde{P}_{ij,h,t}Q_{ij,f,t}\right)\right] \quad \forall ij,f,h,t$$

$$Q^{\mathrm{L}}_{ij,f,t} =$$
(A.7)
$$\sum_{h\in\mathcal{F}} \frac{1}{\tilde{V}_{i,f,t}\tilde{V}_{i,h,t}} \left[R'_{ij,f,h}\left(\tilde{P}_{ij,h,t}Q_{ij,f,t} - \tilde{Q}_{ij,h,t}P_{ij,f,t}\right)\right.$$
$$\left. + X'_{ij,f,h}\left(\tilde{P}_{ij,h,t}P_{ij,f,t} + \tilde{Q}_{ij,h,t}Q_{ij,f,t}\right)\right] \quad \forall ij,f,h,t$$
(A.8)

The term $V^2_{i,f,t,c}$ in the left-hand side of constraint (7) and (10) can be linearized by introducing the variable $V^{\mathrm{sqr}}_{i,f,t,c}$ to represent the square value of voltage magnitude. Furthermore, the terms $P^2_{ij,f,ht,c}$ and $Q^2_{ij,h,t,c}$ in constraint (10) can be linearized introducing the variables $P^{\mathrm{sqr}}_{ij,f,t,c}$ and $Q^{\mathrm{sqr}}_{ij,f,t}$. Thus, the constraint (10) can be rewritten as the linear expression in (A.9). Additionally, (7) can be rewritten as in (A.10).

$$\frac{\left(P^{\mathrm{sqr}}_{ij,f,t,c} + Q^{\mathrm{sqr}}_{ij,f,t,c}\right)}{V^{sqr}_{i,f,t}} \leq \bar{I}^2_{ij} \quad \forall ij,f,t$$
(A.9)

$$V^{\mathrm{sqr}}_{i,f,t,c} - V^{\mathrm{sqr}}_{j,f,t,c} = 2\sum_{h\in\mathcal{F}}\left(R'_{ij,f,h}P_{ij,h,t} + X'_{ij,f,h}Q_{ij,h,t}\right) -$$
$$\frac{1}{V^2_{i,f,t}}\left[\sum_{h\in\mathcal{F}}\left(R'^2_{ij,f,h} + P'^2_{ij,h,t}\right)\cdot\left(P^2_{ij,f,h,t,c} + Q^2_{ij,h,t,c}\right)\right]$$
$$\forall ij,f,h,t \quad (A.10)$$

13

(a) Case II: Contingency at 16:00 hours.

(b) Case III: Contingency at 08:00 hours.

(c) Case V: Contingency at 16:00 hours with EVs.

(d) Case VI: Contingency at 08:00 hours with EVs.

Figure 10: PV curtailment for each case.

On the other hand, $V_{i,f,t,c}^2$ in the right-hand side of constraint (A.10) is approximated based on its estimation, given by $\tilde{V}_{i,f,t,c}$. As mentioned before, the terms $P_{ij,f,ht,c}^2$ and $Q_{ij,h,t,c}^2$ can be linearized introducing the variables $P_{ij,f,t,c}^{\mathrm{sqr}}$ and $Q_{ij,f,t}^{\mathrm{sqr}}$. Finally, the constraint (A.10) can be rewritten as the linear expression in (A.11).

$$V_{i,j,f,t}^{\mathrm{sqr}} - V_{j,f,t}^{\mathrm{sqr}} = 2 \sum_{h \in \mathcal{F}} \left(R'_{ij,f,h} P_{ij,h,t} + X'_{ij,f,h} Q_{ij,h,t} \right) -$$

$$\frac{1}{\tilde{V}_{i,f,t}} \left[\sum_{h \in \mathcal{F}} \left(R'^2_{ij,f,h} + X'^2_{ij,h,t} \right) \cdot \left(P_{ij,f,h}^{\mathrm{sqr}} + Q_{ij,h,t}^{\mathrm{sqr}} \right) \right]$$

$$\forall ij, f, h, t \quad \text{(A.11)}$$

Appendix A.2. Linearization of the BESS model

The nonlinear constraint (21) can be linearized based on the binary varibles $b_{m,t}^{\mathrm{Ch}}$ and $b_{m,t}^{\mathrm{Dis}}$ according to the (A.12). The binary variables are used to represents the operational state of the BESS in charging mode ($b_{m,t}^{\mathrm{Ch}} = 1$) or discharging mode ($b_{m,t}^{\mathrm{Dis}}$). This is enforced by constraints in (A.13) and (A.14), and constraint (A.15) defines the binary nature of variables $b_{m,t}^{\mathrm{Ch}}$ and $b_{m,t}^{\mathrm{Dis}}$.

$$b_{m,t}^{\mathrm{Ch}} + b_{m,t}^{\mathrm{Dis}} \leq 0 \quad \forall m, t \quad \text{(A.12)}$$

$$0 \leq P_{m,t}^{\mathrm{B+}} \leq \overline{P}_m^{\mathrm{B}} \quad \forall m, t \quad \text{(A.13)}$$

$$0 \leq P_{m,t}^{\mathrm{B-}} \leq \overline{P}_m^{\mathrm{B}} \quad \forall m, t \quad \text{(A.14)}$$

$$b_{m,t}^{\mathrm{Ch}}, b_{m,t}^{\mathrm{Dis}} \in 0,1 \quad \forall m, t \quad \text{(A.15)}$$

References

[1] M. Uddin, H. Mo, D. Dong, S. Elsawah, J. Zhu, J. M. Guerrero, Microgrids: A review, outstanding issues and future trends, Energy Strategy Reviews 49 (2023) 101127. doi:https://doi.org/10.1016/j.esr.2023.101127.
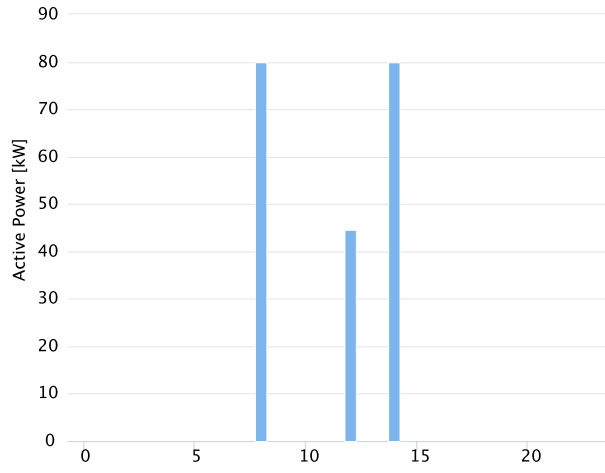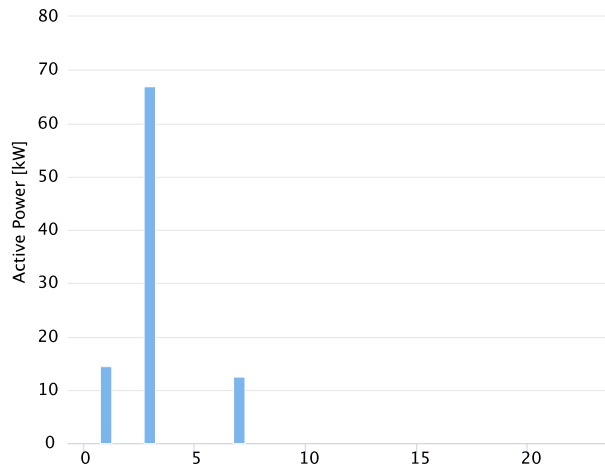
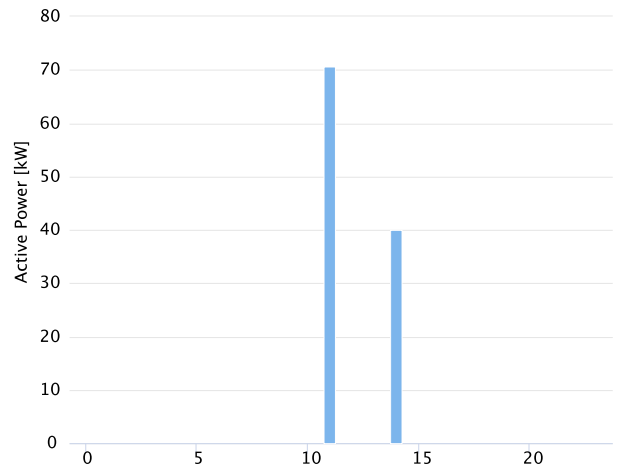(a) Case IV: Without contingencies, including EVs.
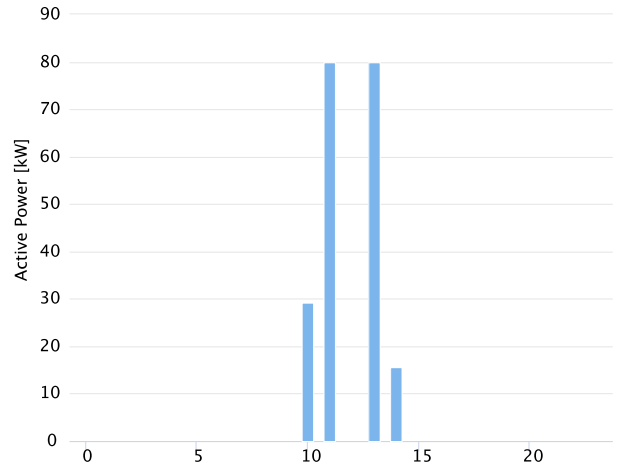
(b) Case V: Contingency at 16:00 hours with EVs.

Figure 11: EV 2 dispatch for each case of study.

(a) EV 1


(b) EV 2

Figure 12: EV dispatch for VI case of study.

[2] M. Farrokhabadi, et al., Microgrid stability definitions, analysis, and examples, IEEE Transactions on Power Systems 35 (1) (2020) 13–29. doi:10.1109/TPWRS.2019.2925703.

[3] X. Yang, Y. Zhang, H. He, S. Ren, G. Weng, Real-time demand side management for a microgrid considering uncertainties, IEEE Transactions on Smart Grid 10 (3) (2019) 3401–3414. doi:10.1109/TSG.2018.2825388.

[4] M. Restrepo, C. A. Cañizares, J. W. Simpson-Porco, P. Su, J. Taruc, Optimization- and rule-based energy management systems at the canadian renewable energy laboratory microgrid facility, Applied Energy 290 (2021) 116760. doi:https://doi.org/10.1016/j.apenergy.2021.116760.

[5] P. P. Vergara, J. M. Rey, J. C. López, M. J. Rider, L. C. da Silva, H. R. Shaker, B. N. Jørgensen, A generalized model for the optimal operation of microgrids in grid-connected and islanded droop-based mode, IEEE Transactions on Smart Grid 10 (5) (2019) 5032–5045. doi:10.1109/TSG.2018.2873411.

[6] P. P. Vergara, J. M. Rey, H. R. Shaker, J. M. Guerrero, B. N. Jørgensen, L. C. P. da Silva, Distributed strategy for optimal dispatch of unbalanced three-phase islanded microgrids, IEEE Transactions on Smart Grid 10 (3) (2019) 3210–3225. doi:10.1109/TSG.2018.2820748.

[7] H. Çimen, N. Bazmohammadi, A. Lashab, Y. Terriche, J. C. Vasquez, J. M. Guerrero, An online energy management system for ac/dc residential microgrids supported by non-intrusive load monitoring, Applied Energy 307 (2022) 118136. doi:https://doi.org/10.1016/j.apenergy.2021.118136.

[8] J. Kim, H. Oh, J. K. Choi, Learning based cost optimal energy management model for campus microgrid systems, Applied Energy 311 (2022) 118630. doi:https://doi.org/10.1016/j.apenergy.2022.118630.

[9] S. Ahmad, M. Shafiullah, C. B. Ahmed, M. Alowaifeer, A review of microgrid energy management and control strategies, IEEE Access 11 (2023) 21729–21757. doi:10.1109/ACCESS.2023.3248511.

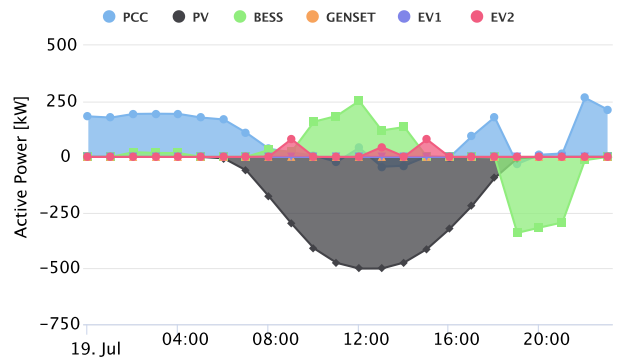[10] N. Bañol Arias, C. Sabillón, J. F. Franco, J. Quirós-Tortós,
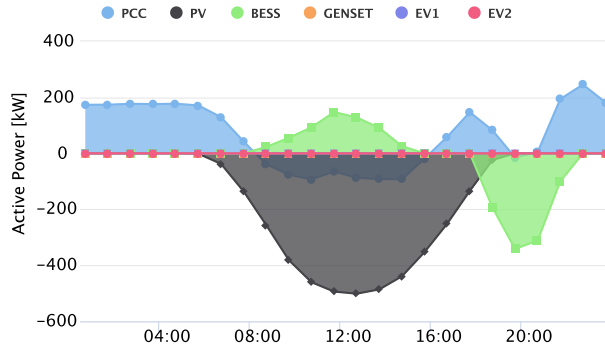
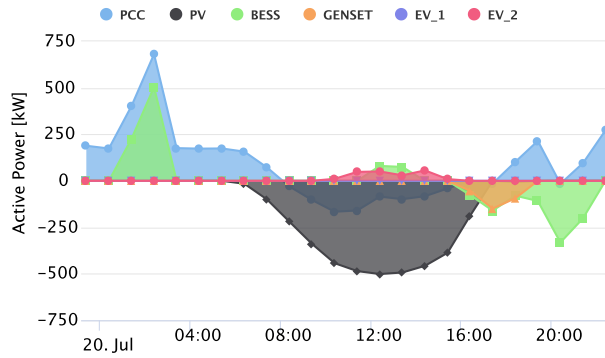(a) Case I: Without contingencies.
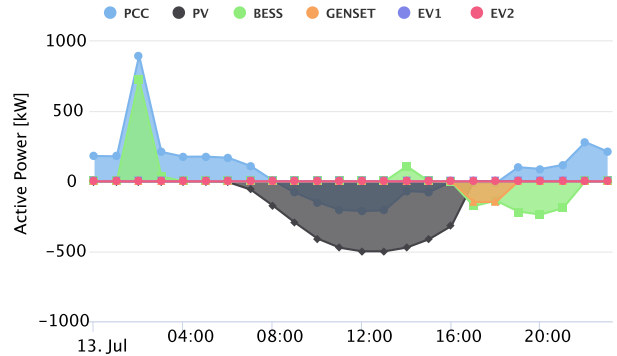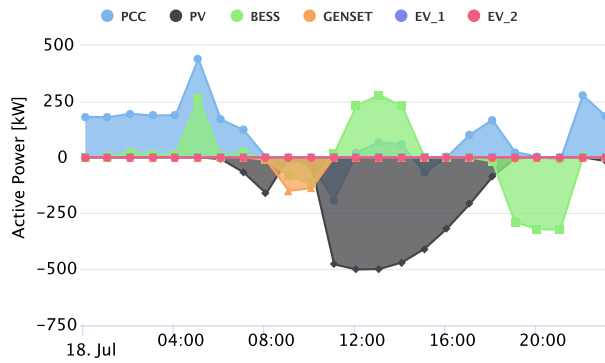
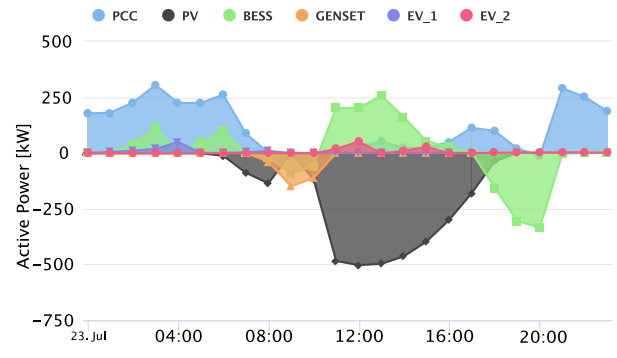(b) Case II: Contingency at 16:00 hours.

(c) Case III: Contingency at 08:00 hours.

(d) Case IV: Without contingencies, including EVs.

(e) Case V: Contingency at 16:00 hours with EVs.

(f) Case VI: Contingency at 08:00 hours with EVs.

Figure 13: Microgrid 24 hours for each case study.

M. J. Rider, Hierarchical optimization for user-satisfaction-driven electric vehicles charging coordination in integrated mv/lv networks, IEEE Systems Journal 17 (1) (2023) 1247–1258. `doi:10.1109/JSYST.2022.3188220`.

[11] I. Calero, C. A. Cañizares, M. Farrokhabadi, K. Bhattacharya, Machine learning-based control of electric vehicle charging for practical distribution systems with solar generation, IEEE Transactions on Smart Grid 15 (3) (2024) 3098–3113. `doi: 10.1109/TSG.2023.3333789`.

[12] S. Guo, P. Li, K. Ma, B. Yang, J. Yang, Robust energy management for industrial microgrid considering charging and discharging pressure of electric vehicles, Applied Energy 325 (2022) 119846. `doi:https://doi.org/10.1016/j.apenergy. 2022.119846`.

[13] K. E. Adetunji, I. W. Hofsajer, A. M. Abu-Mahfouz, L. Cheng, An optimization planning framework for allocating multiple distributed energy resources and electric vehicle charging stations in distribution networks, Applied Energy 322 (2022) 119513. `doi:https://doi.org/10.1016/j.apenergy.2022.119513`.

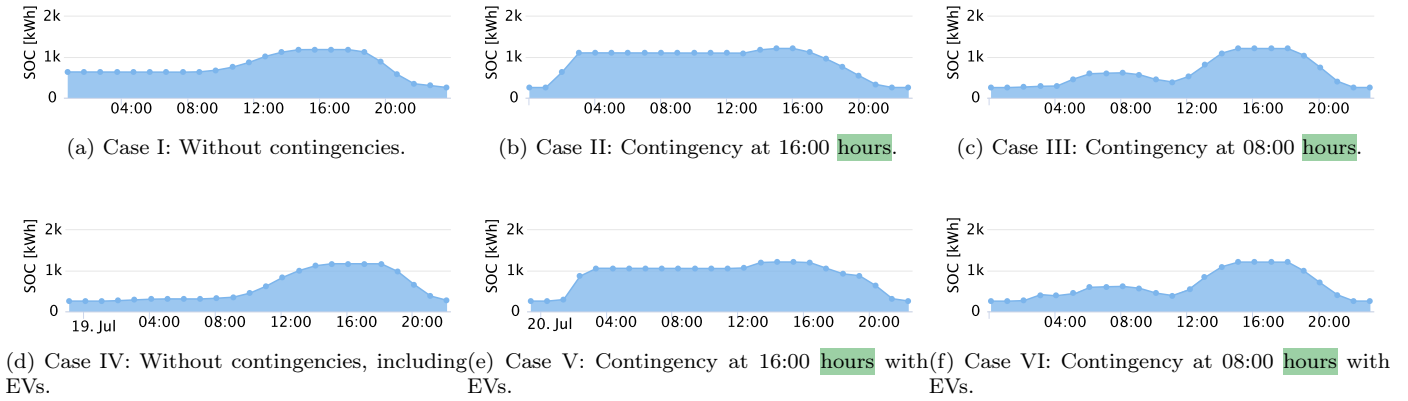[14] H. Masrur, M. Shafie-Khah, M. J. Hossain, T. Senjyu, Multi-

(a) Case I: Without contingencies. (b) Case II: Contingency at 16:00 hours. (c) Case III: Contingency at 08:00 hours.

(d) Case IV: Without contingencies, including EVs. (e) Case V: Contingency at 16:00 hours with EVs. (f) Case VI: Contingency at 08:00 hours with EVs.

Figure 14: BESS's SOC for each case of study.

(a) Case I: Without contingencies. (b) Case II: Contingency at 16:00 hours. (c) Case III: Contingency at 08:00 hours.

(d) Case IV: Without contingencies, including EVs. (e) Case V: Contingency at 16:00 hours with EVs. (f) Case VI: Contingency at 08:00 hours with EVs.
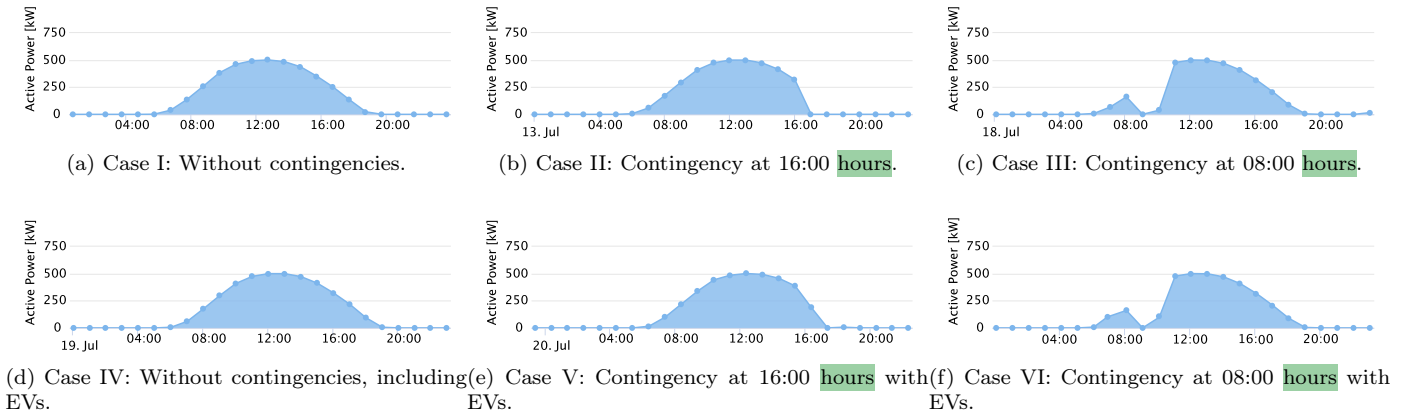
Figure 15: PV generation for each case of study.

energy microgrids incorporating ev integration: Optimal design and resilient operation, IEEE Transactions on Smart Grid 13 (5) (2022) 3508–3518. doi:10.1109/TSG.2022.3168687.

[15] Y. Li, J. Wang, Y. Cao, Multi-objective distributed robust co-operative optimization model of multiple integrated energy systems considering uncertainty of renewable energy and participation of electric vehicles, Sustainable Cities and Society 104 (2024) 105308. doi:https://doi.org/10.1016/j.scs.2024.105308.

[16] X. Zhang, Z. Wang, Z. Lu, Multi-objective load dispatch for microgrid with electric vehicles using modified gravitational search and particle swarm optimization algorithm, Applied Energy 306 (2022) 118018. doi:https://doi.org/10.1016/j.apenergy.2021.118018.

[17] Y. Mei, B. Li, H. Wang, X. Wang, M. Negnevitsky, Multi-objective optimal scheduling of microgrid with electric vehicles, Energy Reports 8 (2022) 4512–4524. doi:https://doi.org/10.1016/j.egyr.2022.03.131.

[18] Z. Ullah, A. U. Rehman, S. Wang, H. M. Hasanien, P. Luo, M. R. Elkadeem, M. A. Abido, Iot-based monitoring and control of substations and smart grids with renewables and electric vehicles integration, Energy 282 (2023) 128924. doi:https://doi.org/10.1016/j.energy.2023.128924.

[19] M. K. Pitchai, P. Narayanan, E. Rajendiran, V. Venkataramani, Iot-enabled ems for grid-connected solar pv-fed dc residential buildings with hybrid hba-dcgnn approach, Energy Conversion and Management 308 (2024) 118361. doi:https://doi.org/10.1016/j.enconman.2024.118361.

[20] S. A. Mansouri, A. Rezaee Jordehi, M. Marzband, M. Tostado-Véliz, F. Jurado, J. A. Aguado, An iot-enabled hierarchical decentralized framework for multi-energy microgrids market management in the presence of smart prosumers using a deep learning-based forecaster, Applied Energy 333 (2023) 120560. doi:https://doi.org/10.1016/j.apenergy.2022.120560.

[21] D. M. Yehia, M. Numair, D.-E. A. Mansour, Novel iot-based droop control for battery soc balancing among multiple micro-grids, IEEE Transactions on Smart Grid 15 (2) (2024) 1304–1316. doi:10.1109/TSG.2023.3304196.

[22] M. S. Abid, H. J. Apon, S. Hossain, A. Ahmed, R. Ahshan, M. H. Lipu, A novel multi-objective optimization based multi-agent deep reinforcement learning approach for microgrid resources planning, Applied Energy 353 (2024) 122029. doi:https://doi.org/10.1016/j.apenergy.2023.122029.

[23] J. A. A. Silva, J. C. López, C. P. Guzman, N. B. Arias, M. J. Rider, L. C. da Silva, An iot-based energy management system for ac microgrids with grid and security constraints, Applied Energy 337 (2023) 120904. doi:https://doi.org/10.1016/j.apenergy.2023.120904.

[24] S. F. Zandrazavi, C. P. Guzman, A. T. Pozos, J. Quiros-Tortos, J. F. Franco, Stochastic multi-objective optimal energy management of grid-connected unbalanced microgrids with renewable energy generation and plug-in electric vehicles, Energy 241 (2022) 122884. doi:https://doi.org/10.1016/j.energy.2021.122884.

[25] L. H. S. Santos, J. A. A. Silva, J. C. López, M. J. Rider, L. C. P. da Silva, Joint optimal sizing and operation of unbal-
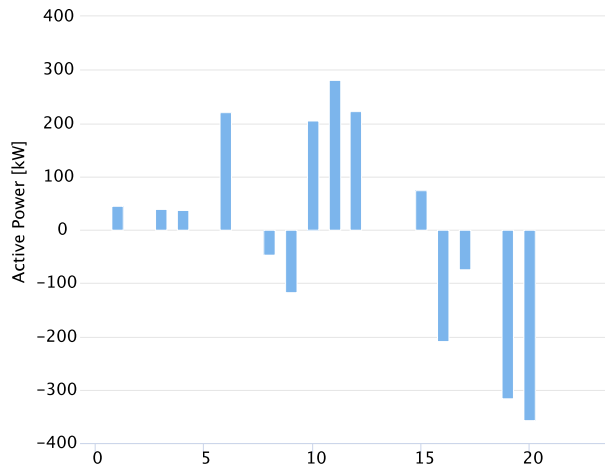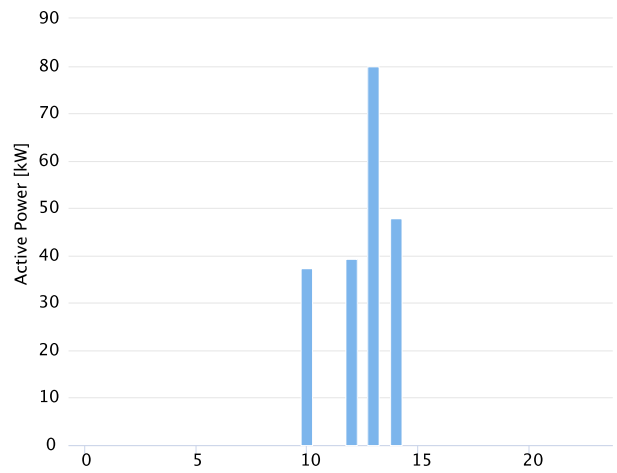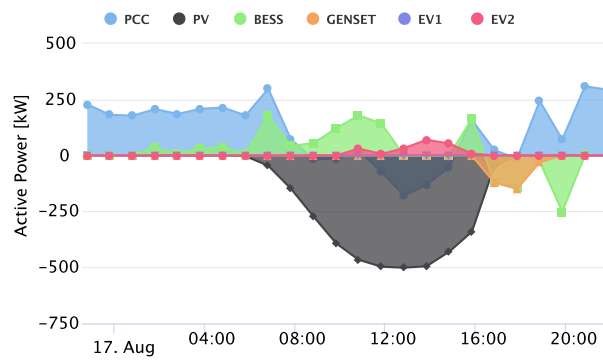
(a) Case VII: Bess dispatch
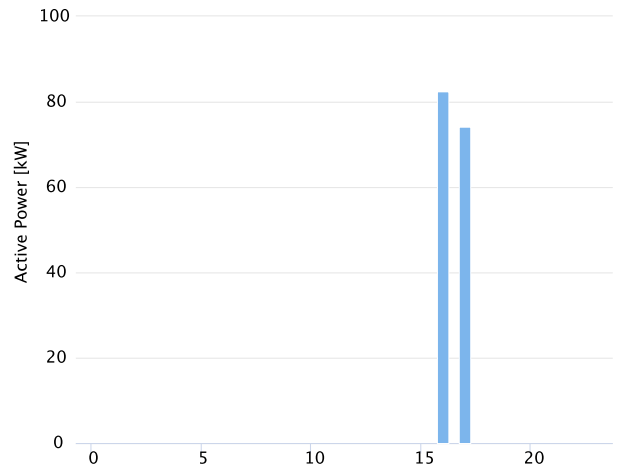
(b) Case VII: Genset dispatch
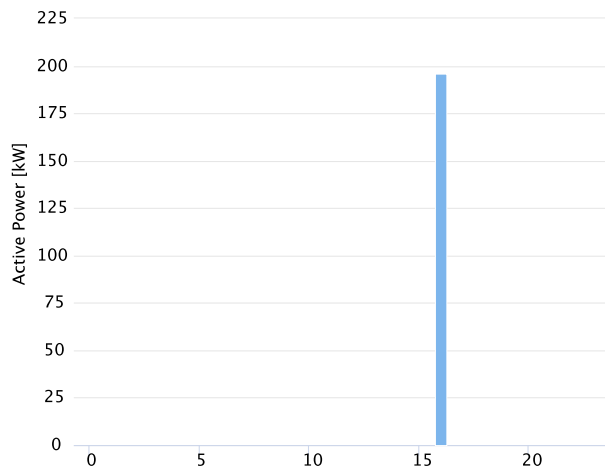
(c) Case VII: PV curtailment

(d) Case VII: EV 2 dispatch

(e) Case VII: Microgrid operation 24 hours

Figure 16: Case VII: Contingencies at 08:00 and 16:00 hours with EVs

anced three-phase ac microgrids using homer pro and mixed-integer linear programming, Journal of Control, Automation and Electrical Systems 35 (2) (2024) 346–360. doi:10.1007/s40313-023-01059-5.

[26] K. Deb, Multi-objective Optimisation Using Evolutionary Algorithms: An Introduction, Springer London, London, 2011, pp. 3–34. doi:10.1007/978-0-85729-652-8_1.
URL https://doi.org/10.1007/978-0-85729-652-8_1

[27] S. Boyd, L. Vandenberghe, Convex optimization, Cambridge university press, 2004.
URL https://web.stanford.edu/~boyd/cvxbook/

[28] G. Chiandussi, M. Codegone, S. Ferrero, F. Varesio, Comparison of multi-objective optimization methodologies for engineering applications, Computers and Mathematics with Applications 63 (5) (2012) 912–942. doi:https://doi.org/10.1016/j.camwa.2011.11.057.

[29] Y. Y. Haimes, L. S. Lasdon, D. A. Wismer, On a bicriterion formulation of the problems of integrated system identification and system optimization, IEEE Transactions on Systems, Man, and Cybernetics SMC-1 (3) (1971) 296–297. doi:10.1109/TSMC.1971.4308298.

[30] I. Docker, Docker Compose, version X.Y.Z, Accessed: 2023-07-01 (2023).
URL https://docs.docker.com/compose/

[31] I. Sysoev, NGINX: High Performance Load Balancer, Web Server, and Reverse Proxy, NGINX, Inc., accessed: 2023-07-01 (2024).
URL https://nginx.org/

[32] J. Forrest, et al., coin-or/cbc: Release releases/2.10.11 (Oct. 2023). doi:10.5281/zenodo.10041724.

[33] M. L. Bynum, G. A. Hackebeil, W. E. Hart, C. D. Laird, B. L. Nicholson, J. D. Siirola, J.-P. Watson, D. L. Woodruff, Pyomo–optimization modeling in python, 3rd Edition, Vol. 67, Springer Science & Business Media, 2021.

[34] W. E. Hart, J.-P. Watson, D. L. Woodruff, Pyomo: modeling and solving mathematical programs in python, Mathematical Programming Computation 3 (3) (2011) 219–260.

[35] Oracle Corporation, MySQL: The world's most popular open source database, Oracle Corporation, version 8.0 (2024).
URL https://dev.mysql.com/doc/

[36] A. Ronacher, Flask: A python microframework, version 3.0.x, Accessed: 2023-07-01 (2024).
URL https://flask.palletsprojects.com/en/3.0.x/

[37] Typhoon HIL, Typhoon HIL Control Center, accessed: 2023-08-03 (2024).
URL https://www.typhoon-hil.com/products/software/)

[38] Typhoon HIL, Typhoon HIL Application Programming Interface, accessed: 2023-08-03 (2024).
URL https://www.typhoon-hil.com/documentation/typhoon-hil-typhoontest-library/#

[39] Google LLC, Angular: The modern web developer's platform, Google LLC, version 16.0 (2024).
URL https://angular.dev/

[40] ANEEL, Ranking das Tarifas, accessed on Jun. 19 (2024).
URL https://portalrelatorios.aneel.gov.br/luznatarifa/rankingtarifas

[41] L. A. Zaneti, N. B. Arias, M. C. de Almeida, M. J. Rider, Sustainable charging schedule of electric buses in a university campus: A rolling horizon approach, Renewable and Sustainable Energy Reviews 161 (2022) 112276. doi:https://doi.org/10.1016/j.rser.2022.112276.

[42] J. A. A. Silva, J. C. López, N. B. Arias, M. J. Rider, L. C. da Silva, An optimal stochastic energy management system for resilient microgrids, Applied Energy 300 (2021) 117435. doi:https://doi.org/10.1016/j.apenergy.2021.117435.

Appendix B. Work Plan and Schedule

To accomplish the activities of this Master's degree project adequately, solid theoretical knowledge in the area of microgrids and power systems was necessary. This master's project began in the first semester of 2023. The courses that were taken in the first two semesters were those shown in Table B.3.

Table B.3: Courses taken to complete required credits.

1st	IT509-A - Stochastic Processes for Engineering (Concept B)
	IT511-A - Energy Operation of Electric Power Systems (Concept A)
2nd	IT306-Q - Topics in Electric Power Systems III: Optimization Applied to Electric Power Distribution Systems (Concept A)
	IT306-HH - Topics in Electric Power Systems III: Energy Storage Systems (Concept A)

The stages of the master's works are shown below.

Stage 01 Taking courses to fulfill the credit requirements.

Stage 02 Continuation of courses for required credits and introduction to the MERGE project.

Stage 03 Learning and understanding the CAMPUSGRID microgrid mathematical model using Python and Pyomo.

Stage 04 Implementation of the mathematical model with the inclusion of linearizations, contingencies and scenarios using Pyomo.

Stage 05 Gaining knowledge of the backend (Flask API and database) and frontend (Angular) technologies.

Stage 06 Preparing study cases for 24-hours simulations with software Typhoon HIL604.

Stage 07 Preparation for the qualification exam.

Stage 08 Simulations with hardware Typhoon HIL604 in the Smart Grids Laboratory (LABREI), a rolling horizon approach and PV forecasting will be included.

Stage 09 Writing and preparation of the master thesis.

Stage 10 Defending the master's thesis.

The schedule of the completed and planned stages is in Table B.4. In addition, two papers were developed and submitted for conferences.

1. **Gerenciamento de Energia em Tempo Real da Microrrede LABREI**, Published in "Congresso Brasileiro de Energia Solar", Natal RN, 2024.
Authors: Jéssica Alice A. Silva, Derian C. Tairo, Juan Camilo López, Guilherme S. Chagas, Marcos J. Rider, Luiz C. P. da Silva.

Table B.4: Scheduled and project status

Stage	1st 2023	2nd 2023	1st 2024	2nd 2024
01	■			
02		■		
03		■		
04		■		
05			■	
06			■	
07			■	
08				■
09				■
10				■

Done	To do

2. **Stochastic Optimization of Energy Resources in Smart Homes**, Accepted to the IEEE ANDESCON, Cusco - Perú, 2024.
Authors: Jéssica Alice A. Silva, Derian C. Tairo, Guilherme S. Chagas, Marcos J. Rider.